

# Evolution of Magnetic Domain Morphology in Co/Pt Thin Films

Andrew Westover

A senior thesis submitted to the faculty of  
Brigham Young University  
in partial fulfillment of the requirements for the degree of

Bachelor of Science

Dr. Karine Chesnel, Advisor

Department of Physics and Astronomy

Brigham Young University

August 2012

Copyright © 2012 Andrew Westover

All Rights Reserved

## ABSTRACT

### Evolution of Magnetic Domain Morphology in Co/Pt Thin Films

Andrew Westover  
Department of Physics and Astronomy  
Bachelor of Science

Cobalt (Co)/Platinum (Pt) thin films form into magnetic domains on a microscopic scale that align perpendicular to the film. This property makes them of particular interest for usage in ultra-high-density magnetic storage. Vibrating Sample Magnetometry (VSM), Extraordinary Hall Effect Magnetometry (EHE), and Magnetic Force Microscopy (MFM) was used to study the magnetic domain periodicity and hysteresis behavior of Co/Pt thin films with variable Co thickness ranging from 4Å to 60Å. As the thickness of Co increases, the domain periodicity increases and the relative amount of hysteresis decreases. The effect of applying major and minor magnetization loops of varying intensities to these samples was also studied, using MFM to observe the domain morphologies at remanence. The MFM images show that the domain morphology can vary from a long strip state to a bubble state depending on the intensity of magnetization loop applied.

Keywords: Co/Pt thin films, magnetic domains, VSM, MFM, EHE, domain morphology, hysteresis, remanence, magnetization loop

## ACKNOWLEDGMENTS

I would like to thank Dr. Karine Chesnel for her invaluable help in gathering, analyzing and interpreting the data, as well as her great help in editing. Her constant support has not only greatly aided in making this work, but has made it possible. I would also like to acknowledge the work of Phillip Salter who designed the Magnetic Image Analyzer program that the bulk of the data analysis much simpler. My thanks also goes out to Yanping Cai, Kelsey Hatch, and Matthew Rytting also provided a great deal of help in gathering data when I wasn't able to collect it all myself. Finally I would like to thank my Parents for their constant encouragement and support.

## Table of Contents

<b>Abstract</b> .....	<b>i</b>
<b>Acknowledgements</b> .....	<b>ii</b>
<b>Table of Contents</b> .....	<b>iv</b>
<b>Table of Figures</b> .....	<b>vi</b>
<b>1. Introduction</b> .....	<b>1</b>
<b>2. Ferromagnetic Materials</b> .....	<b>2</b>
2.1. Ferromagnetism .....	2
2.2. Co/Pt thin films .....	4
<b>3. Magnetic Characterization</b> .....	<b>6</b>
3.1. Extraordinary Hall Effect Magnetometer (EHE) .....	6
3.2. Vibrating Sample Magnetometer (VSM) .....	8
3.3. Magnetic Force Microscopy (MFM) .....	8
3.3.1. Basics of MFM .....	8
3.3.2. In-situ MFM .....	10
3.3.3. Statistical Magnetic Image Analyzer (MIA) .....	11
<b>4. Magnetization Loops</b> .....	<b>13</b>
4.1. Major loops .....	13
4.2. Minor loops .....	14
4.3. Summary .....	20
<b>5. In-Situ MFM Study</b> .....	<b>21</b>
5.1. Major loop in-situ MFM images .....	21
5.2. Major loop in-situ quantitative analysis .....	22
5.2.1. Magnetization loop reconstruction .....	22
5.2.2. Number of domains .....	24
5.3. Minor loop.....	25
5.4. Summary .....	27
<b>6. Remanence MFM Study</b> .....	<b>29</b>
6.1. Remnant domain morphologies in 8Å sample .....	29
6.2. Remnant domain morphologies across thickness .....	33
6.3. Analysis of remnant MFM images across thickness .....	42

6.3.1. Minor loop Peak position vs. saturation .....	42
6.3.2. Number of domains vs. $t_{C_0}$ .....	42
6.3.3. Number of domains vs. $t_{C_0}$ and $H_L$ .....	43
<b>7. Conclusion .....</b>	<b>46</b>
<b>Bibliography .....</b>	<b>47</b>

## Table of Figures

Figure 2.1: Magnetization Loop .....	3
Figure 2.2: Co/Pt Thin Films .....	5
Figure 3.1: Hall Effect Setup .....	7
Figure 3.2: AFM and MFM Images .....	9
Figure 3.3: In-situ MFM Setup .....	10
Figure 3.4: In-situ MFM Field Calibration .....	11
Figure 4.1: Co/Pt Thin Films Magnetization Loops .....	13
Figure 4.2: $H_s$ and $H_n$ .....	14
Figure 4.3: 60Å Magnetization Loops .....	15
Figure 4.4: 40Å Magnetization Loops .....	16
Figure 4.5: 31Å Magnetization Loops .....	16
Figure 4.6: 25Å Magnetization Loops .....	17
Figure 4.7: 16Å Magnetization Loops .....	17
Figure 4.8: 12Å Magnetization Loops .....	18
Figure 4.9: 8Å Magnetization Loops .....	18
Figure 4.10: 4Å Magnetization Loops .....	19
Figure 4.11: Comparison of $H_t$ with $H_s$ and $H_n$ .....	20
Figure 5.1: 8Å In-situ MFM Magnetization Loop .....	22
Figure 5.2: Magnetization Loop Reconstruction .....	23
Figure 5.3: Number of Domains .....	24
Figure 5.4: In-situ MFM Minor Magnetization Loop .....	26
Figure 5.5: Minor Loop Number of Domains .....	27
Figure 6.1: Experimental Process .....	29
Figure 6.2: 8Å Remnant MFM Images .....	30
Figure 6.3: 60Å Remnant MFM Images .....	34
Figure 6.4: 40Å Remnant MFM Images .....	35
Figure 6.5: 31Å Remnant MFM Images .....	36
Figure 6.6: 25Å Remnant MFM Images .....	37
Figure 6.7: 16Å Remnant MFM Images .....	38
Figure 6.8: 12Å Remnant MFM Images .....	39
Figure 6.9: 8Å Remnant MFM Images .....	40

Figure 6.10: 4Å Remnant MFM Images .....	41
Figure 6.11: Comparison of $H_p^L$ and $H_s$ .....	42
Figure 6.12: Number of Domains at $H_p^L$ vs. $t_{Co}$ .....	43
Figure 6.13: Number of Domains vs. $H_L$ and $t_{Co}$ .....	44

# Chapter 1

## Introduction

With the development of computers, ferromagnetic materials gained great importance as a digital storage device. Within a ferromagnetic material, the magnetic moments of thousands of neighboring atoms tend to align in the same direction forming a magnetic domain. Individual domains can then be used to store bits of information. In certain materials these domains were found to exhibit perpendicular magnetic anisotropy. Perpendicular magnetic anisotropy is a property where the domains tend to align perpendicular to the film. In the late 1970s, it was discovered that Cobalt (Co) / Platinum (Pt) multilayers exhibited perpendicular magnetic anisotropy. The advantage of these films was that the domains produced were several orders of magnitude smaller than those in previously discovered materials. This provided greatly increased data storage potential.

I used Vibrating Sample Magnetometry (VSM), Extraordinary Hall Effect Magnetometry (EHE), and Magnetic Force Microscopy (MFM), to study the effect of Co thickness on the magnetization loops, and remnant domain morphology with different magnetization loops. Using these techniques I obtained detailed information about the morphological differences between different sample thickness and previously applied field. Understanding these morphological differences is important for understanding how these samples can be applied to data storage.

# Chapter 2

## Ferromagnetic Materials

### 2.1 Ferromagnetism

Magnetism in materials arises from the spin and orbital angular momenta carried by electrons. The net magnetic moment of an atom is the sum of the net magnetic moments of all of the electrons in the atom. In general, the orbital magnetic moment of an atom is almost negligible in comparison to the spin magnetic moment. In many atoms the spins of neighboring atoms pair up, canceling each other out on an atomic scale. In order for an atom to have a spin magnetic moment, it must have electrons with unpaired spins. (See [1] Chapter 4 and 5)

Ferromagnetism occurs when the spins in a material are coupled together. This means that the magnetic moment of neighboring atoms tend to all point in the same direction. Groups of atoms with coupled spins are called magnetic domains. In most materials, the magnetic moments of neighboring atoms can point in any direction, leading to zero net magnetization, unless an external magnetic field is applied. Ferromagnetic materials, on the other hand, can have a non-zero magnetization even when there is no external magnetic field applied because of magnetic domains. (See [2] chapter 6)

A common way to characterize the magnetic behavior of a material is to measure its magnetization loop. A magnetization loop is obtained by measuring the net magnetization with applied magnetic field. The loop consists of an ascending branch and a descending branch. The ascending branch corresponds to starting the measurement at some negative

field value,  $-H$ , and increasing it to the same positive value,  $H$ . The descending branch starts at a positive field value,  $H$ , and is decreased to the same negative field value,  $-H$ . There are two types of magnetization loops: major and minor. A major loop means that saturation was achieved before reversing the field; a minor loop means that the field was reversed before saturation was reached. Saturation denotes the field value where all of the magnetic domains in the material align with the applied field. This gives the maximum possible net magnetization.

## Magnetization Loop

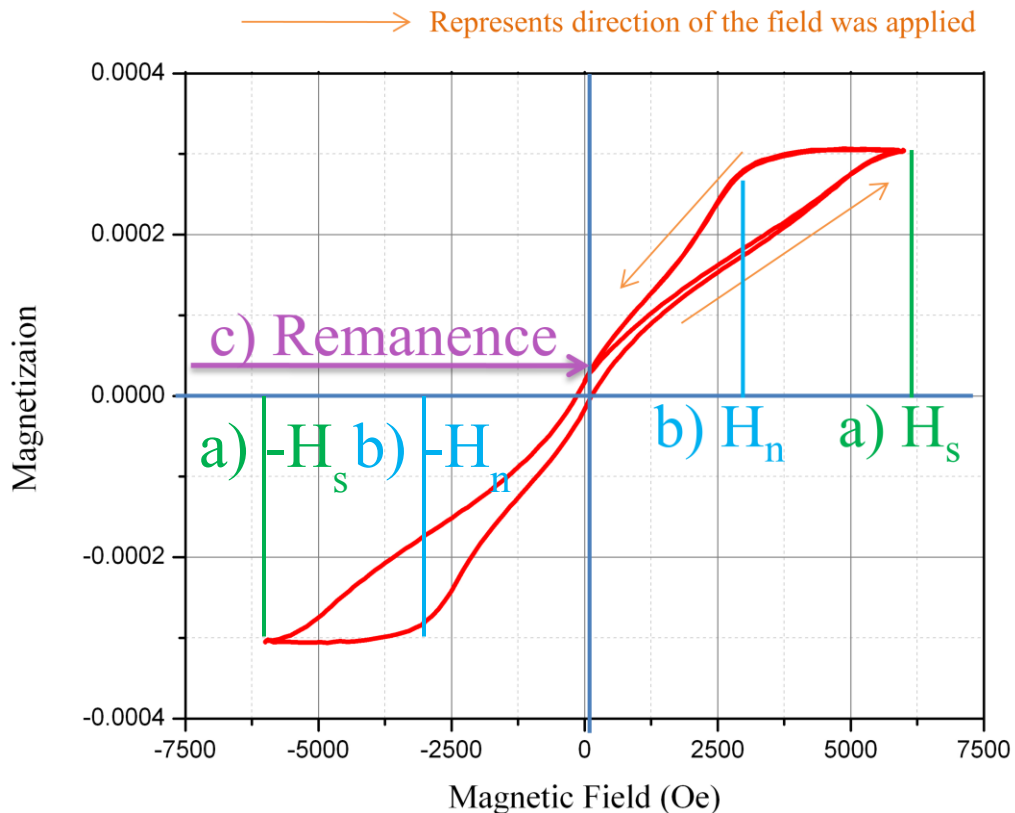


Figure 2.1: A representation of a magnetization loop showing the key points. a)  $H_s$ : the point at which all the domains align with the field. This is also the point with the largest net magnetic moment. b)  $H_n$ : The point where saturated domains start to reverse direction. c) Remanence: the point where there is no net applied field.

Each branch of a major magnetization loop consists of three major points: saturation, nucleation, and remanence (Points a, b, and c respectively on figure 2.1). I will use  $H_n$  to refer to the nucleation field, and  $H_s$  to refer to the saturation field. The ascending branch starts at  $-H_s$ . Once  $H_n$  is reached, domains aligned opposite the field start to appear and propagate through the sample. Remanence occurs when the applied field reaches zero. The ascending branch is completed by positively saturating the material. The descending branch is symmetrical with the ascending branch. It starts at  $+H_s$  and ends at  $-H_s$ . In ferromagnetic materials, it is possible to have a non-zero magnetization at remanence. A minor magnetization loop will only have remanence.

There are two types of magnetization loops: major and minor. A major loop means that saturation was achieved before reversing the field; a minor loop means that the field was reversed before saturation was reached.

## 2.2 Co/Pt thin films

The structure of the Co/Pt thin films used in this study is shown in figure 2.2. The films are grown on a Si substrate, and includes a buffer layer made of 200 Å of Pt, a Co/Pt multilayer, and a capping layer made of 23 Å of Pt to prevent oxidation. The multilayers in our samples consist of 50 bilayers of Co/Pt. The bilayers are made of a Co layer with thicknesses ranging from 4Å to 60Å and a Pt layer 7 Å in thickness. I will use  $t_{Co}$  to denote Co thickness. They are of particular interest due to their property of exhibiting perpendicular magnetic anisotropy, the tendency for magnetic domains to align perpendicular to the film.

Since their discovery, there has been much interest in the magnetic properties of these [Co/Pt] thin films. There have been many studies on the effect of the number of bilayers of Co/Pt [3], the relative thicknesses of Co and Pt [4, 5, 6, 7], the domain morphology without a magnetic field applied [7, 8], and the evolution of the domain morphology as an external magnetic field is applied [3, 9, 10, 11].

I have investigated the effect of  $t_{\text{Co}}$  on magnetic behavior. Although there have been some studies that investigate the effect of thickness, most of these studies were done on Co/Pt thin films with  $t_{\text{Co}}$  ranging from  $2\text{\AA}$  to  $20\text{\AA}$ , with the majority studying  $t_{\text{Co}} < 4\text{\AA}$ . My study expands on previous studies, providing an in depth magnetic characterization for  $t_{\text{Co}}$  not previously studied.

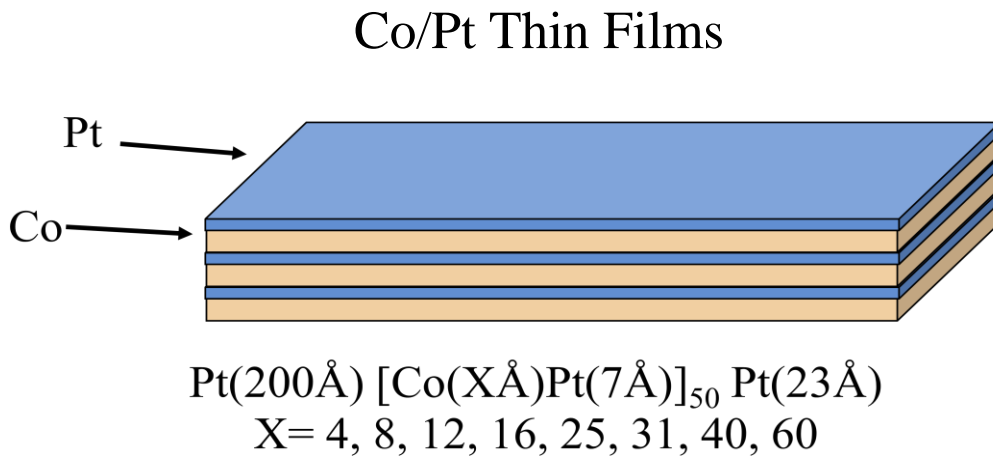


Figure 2.2: A representation Co/Pt thin films. The orange layer represents the Co, and the blue layer represents Pt. The thin films are a made of many bilayers of Co/Pt. The samples studied are organized according to the formula. They have a base layer of  $200\text{\AA}$  of Pt, 50 bilayers of Co/Pt with a variable thickness  $x$  for Co,  $7\text{\AA}$  of Pt, and a capping layer of  $23\text{\AA}$  of platinum.

# Chapter 3

## Magnetic Characterization

I used Extraordinary Hall Effect Magnetometry (EHE) and Vibrating Sample Magnetometry (VSM) to measure magnetization loops, and Magnetic Force Microscopy (MFM) to observe the magnetic domain morphology.

### 3.1 Extraordinary Hall Effect Magnetometer (EHE)

When an electric charge moves in the presence of an external magnetic field it experiences a force, called the Lorentz force perpendicular to both the direction of the velocity ( $v$ ) of the electric charge ( $q$ ), and the direction of the magnetic field ( $B$ ):

$$F_{Lorentz} = qv \times B$$

When a conductive material is placed in a magnetic field, and a current is run through the sample, the charges flow across the sample perpendicular to both the direction of the current and the magnetic field, building up on the edges. This causes a voltage across the sample. This phenomenon is called the Hall effect

In simple conducting materials the magnetic field in the Lorentz force is solely due to the externally applied magnetic field. In magnetic materials however, the magnetic field in the Lorentz force has a component given by the externally applied field, and a component that comes from the magnetization of the sample [12] the effective voltage then has an extra component called the extraordinary Hall effect. The following equation represents this extraordinary component.

$$H_e = H_0 + 4\pi M\alpha$$

$H_e$  is the effective magnetic field, and  $H_0$  is the externally applied field,  $M$  is the magnetization of the sample, and  $\alpha$  is proportionality constant. This equation means that there is a component of the hall voltage that is proportional to the magnetic moment of the material. This is called the extraordinary Hall effect.

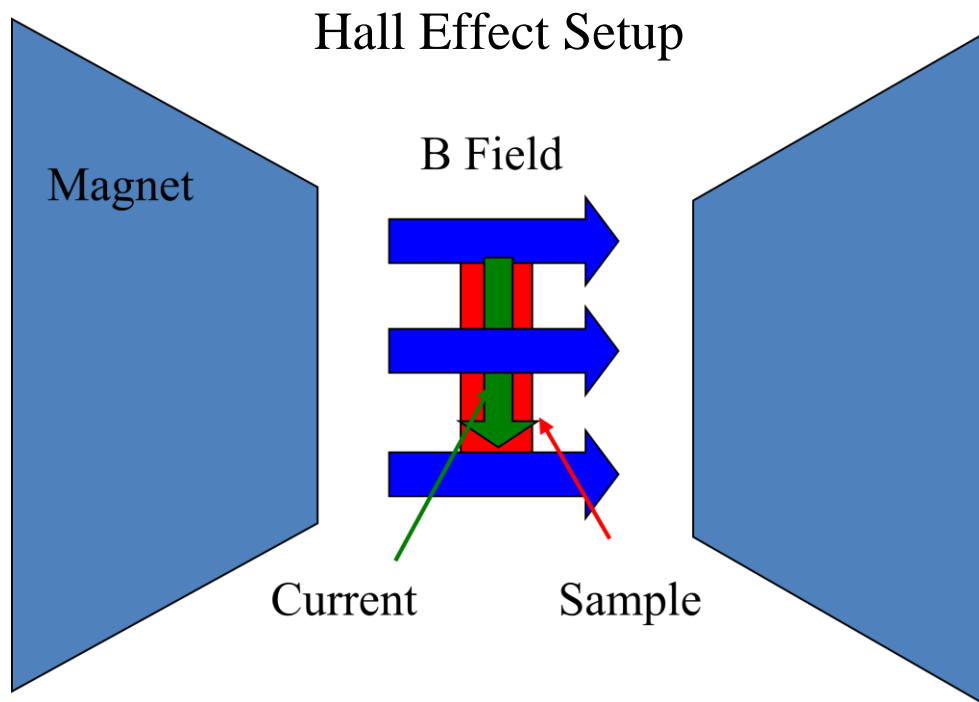


Figure 3.1: Extraordinary Hall Effect Magnetometer Setup. Red is the sample Dark Green represents the direction of the current. Blue represents the direction of the magnetic field. When a current is run through a conductive sample in the presence of a magnetic field, the electrons move across the sample according to Lorentz's law forming a voltage across the sample. This voltage is called the hall voltage.

In the case of Co/Pt thin films the component proportional to the magnetization is significantly greater than that of the externally applied field. So for these Co/Pt thin films the Hall voltage is approximately proportional to the magnetization of the sample. Our extraordinary Hall effect magnetometer setup can be seen in figure 3.1.

## 3.2 Vibrating Sample Magnetometer (VSM)

The VSM operates using Faraday's Law

$$V = -\frac{d\phi}{dt}$$

where  $V$  is the electromagnetic potential induced in a wire, and  $\phi$  is the magnetic flux. The magnetic flux is a quantity that describes how intense the magnetic field is in a given area. When there is a change in magnetic flux within a loop of wire it creates a voltage, which in turn induces a current in the wire. In the VSM, a magnetic sample rapidly oscillates inside of a wire loop. This causes a current to flow in the loop proportional to the magnetic moment of the sample. A magnetization loop can then be measured by changing the externally applied magnetic field.

## 3.3 Magnetic Force Microscopy (MFM)

### 3.3.1 Basics of MFM

Magnetic Force Microscopy is a derivative of Atomic Force Microscopy (AFM). AFM is a scanning technique that is somewhat like running ones finger lightly over a flat surface. Doing so, one can tell when there is a dent, or a mound etc. Effectively, one can measure

the topography of the surface. AFM works by having a cantilever with a sharp pointed tip on the end. When the tip is brought within a few nanometers of the surface, it can be used to measure the inter-atomic forces between the tip and the surface. The tip is then scanned across the sample, which forms a topographical image.

In MFM, the tip is coated with a ferromagnetic material typically 5-10 nm in thickness, and then magnetized, giving the tip its own magnetic moment. MFM works by first taking an AFM scan, then lifting up several nanometers above the sample and scanning over the sample following the previously scanned topography. What remains is a pure magnetic interaction between the magnetic moment of the tip, and the magnetic stray field of the sample [13]. The resulting image arises from the gradient in the magnetic stray field. An example of corresponding AFM and MFM images can be seen in figure 3.2.

## AFM and MFM Images

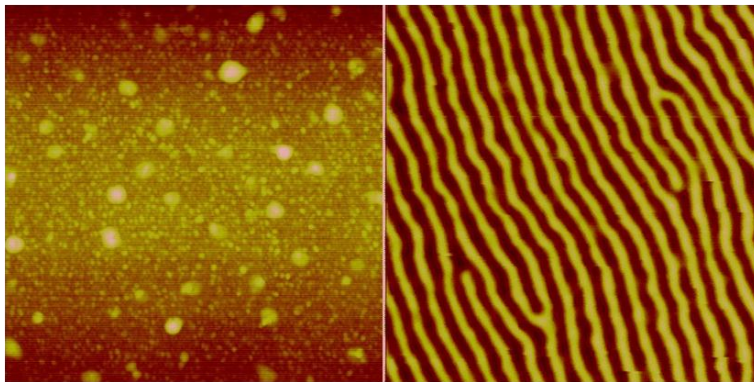


Figure 3.2: On the left is an example of an AFM topography scan. On the right is the corresponding MFM domain morphology scan at the same location.

### 3.3.2 In-situ MFM

MFM is most commonly done with no magnetic field applied, but with the proper setup MFM can also be done in the presence of an external magnetic field [13].

So that I could perform in-situ MFM on the Co/Pt samples I implemented such a setup. The basic idea is similar to that implemented by Bran et al. [10]. Figure 3.3 shows my in-situ MFM setup. I have a linear z stage that allows me to adjust the distance between a set of permanent magnets, and the sample.

### In-situ MFM Setup

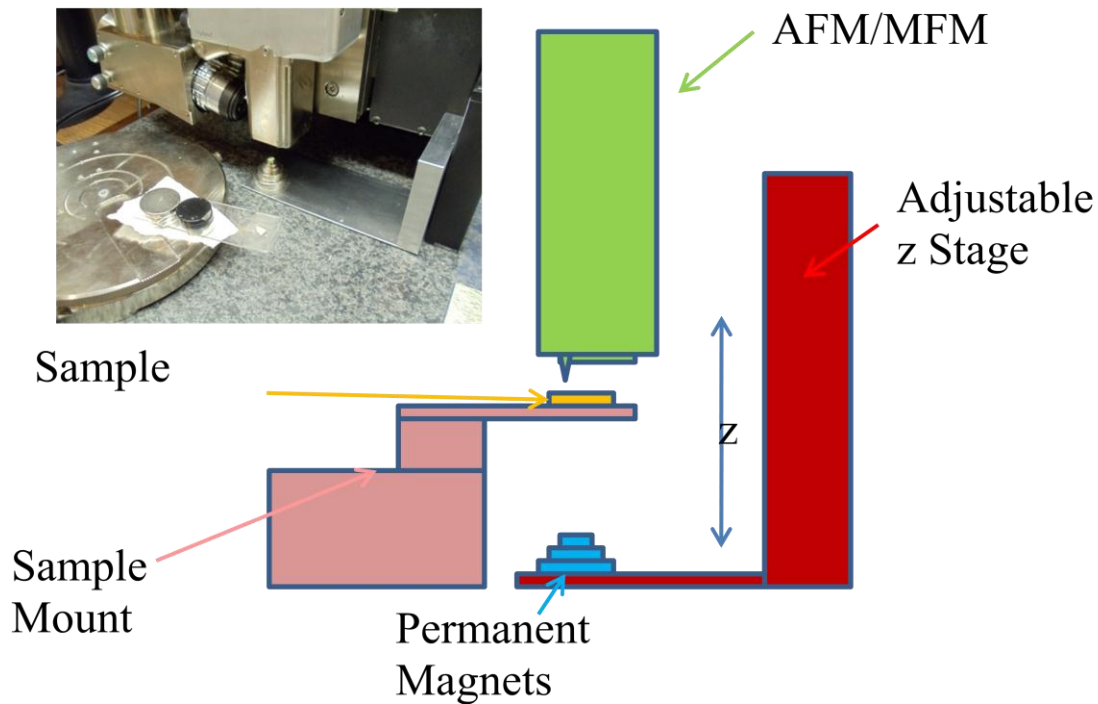


Figure 3.3: The inset in the top left is a picture of our actual In-Situ MFM setup. The diagram illustrates all the key parts. The field affecting the sample can be adjusted by bringing the permanent magnets closer, or farther away from the sample.

stage. When the magnets are brought closer to the sample, the increase is exponential, as would be expected for a magnetic material. Figure 3.4 also reveals one of the limitations

of this in-situ MFM setup. This maximum field that can be applied is about 6000 Oe. Unfortunately, this field can only saturate 2 of our 8 samples, severely limiting the techniques potential usefulness for this study.

## In-situ MFM Field Calibration

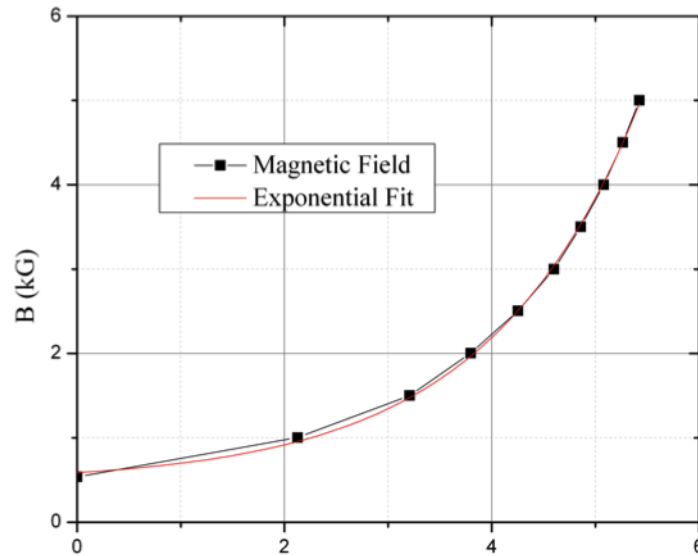


Figure 3.4: The magnetic field as a function of height read on the In-situ MFM z stage. The red curve is a fit of the data.

### 3.3.2 Statistical Magnetic Image Analyzer (MIA)

Magnetic domain morphologies in Co/Pt thin films are characterized by large quantities of domains aligned perpendicularly in and out of the film. In order to provide quantitative analysis in addition to the qualitative analysis, Phillip Salter and I developed a program to analyze magnetic images. The program has 4 basic steps.

It first creates a grayscale version of the MFM image, converting all pixels to +1 spin for spin up, -1 for spin down. This uses a midpoint  $a_0$  as the delimiter.

Second, the program compiles a list of all the domains in the sample and their sizes in pixels. It does this by scanning the sample from right to left, and top to bottom, marking groups of neighboring pixels in the same direction.

Third, the program uses the list of domains to calculate for both spin up and spin down the total number of pixels, denoted by  $N_+$  and  $N_-$ ; the total number of domains,  $D_+$  and  $D_-$ ; and the average domain size,  $S_+$  and  $S_-$ .

Finally, it calculates the net magnetic moment of the sample by taking the total number of positive pixels subtracting the total number of negative pixels, and then dividing by the total number of pixels in the image as seen in the following equation.

$$M = \frac{N_+ - N_-}{N_+ + N_-}$$

There is one limitation when performing the net magnetization calculation with in-situ MFM images. The AFM/MFM software automatically tries to provide each image with the maximum amount of contrast possible. It does this by adjusting the midpoint  $a_0$ , or the contrast between light and dark. Thus in order to get a correct reading for the net magnetization  $a_0$  must be manually adjusted to correct for this artifact.

# Chapter 4

## Magnetization Loops

### 4.1 Major loops

The general magnetization behavior of Co/Pt thin films has been documented extensively [4, 5, 7, 9, 11, 14]. Although there has been much research done into the overall magnetization behavior, I extend these studies to films with larger thicknesses than previously studied.

### Co/Pt Thin Films Magnetization Loops

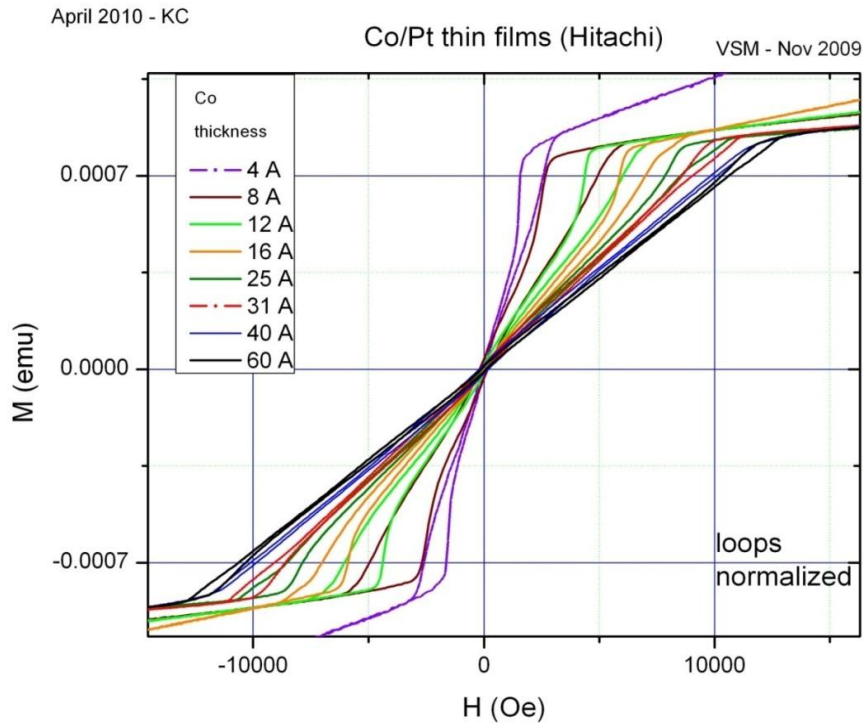


Figure 4.1. The major magnetization loops for each of our samples, going from the 4 Å in purple, to the 60 Å in black. The thinner samples have a large amount of hysteresis, and the thicker samples have a small amount of hysteresis.

The magnetization loops for our samples can be seen in figure 4.1. There are two major regions that each of our samples exhibits. First a large linear reversible region, and second an irreversible opening. In this case *reversible* means that the ascending and descending branches of the magnetization loop are mostly the same. *Irreversible* means that the ascending and descending branches do not meet up. As the thickness of the Co increases, the extent of this larger linear region increases, and the irreversible region decreases. Thus the thicker films have a small amount of hysteresis, and the thinner films have a large amount of hysteresis. This can also be seen in figure 4.2. Figure 4.2 shows the saturation point,  $H_s$ , and the nucleation point,  $H_n$ , as a function of  $t_{Co}$ . The result that thicker samples have less and less hysteresis is consistent with the results reported by Labrune [4], Zeper [6], and Hellwig [14].

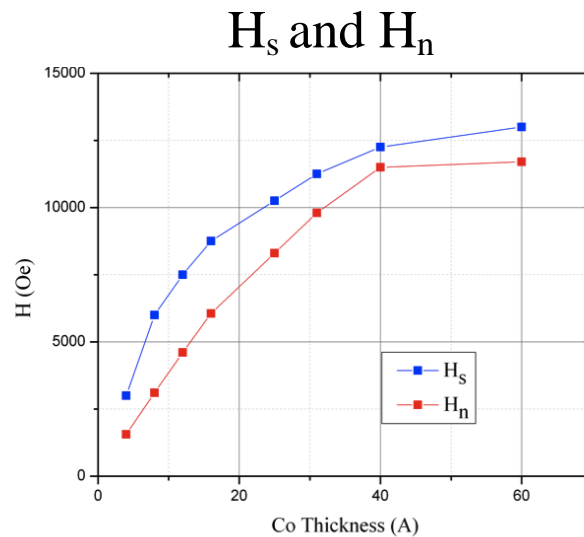


Figure 4.2. The black curve represents the saturation point as a function of Co thickness. The red curve represents the nucleation point as a function of Co thickness.

The overall behavior of both  $H_s$  and  $H_n$  appears to be asymptotic, meaning that they appear to be converging towards a single value. When it reaches this value the saturation and nucleation points will be independent of  $t_{Co}$ .

## 4.2 Minor loops

Although it is obvious that there is both a linear reversible region, and an irreversible opening in the loop, major loops alone are not enough to determine the exact point at which this transition occurs. In order to determine exactly where this transition occurs, I performed a series of minor loops on each sample. The minor loops for each sample are shown in Figures 4.3-4.10.

The *s* shape visible in some graphs is most probably not due to the sample, but due to contamination in the sample holder. In each of these sets of minor loops, one can clearly see that some minor loops are completely closed, and some are open towards  $H_s$ . For the thicker samples,  $t_{Co} > 25\text{\AA}$ , this transition is extremely clear. For the thinner samples,  $t_{Co} < 25\text{\AA}$ , however this transition appears to be more gradual.

### 60Å Magnetization Loops

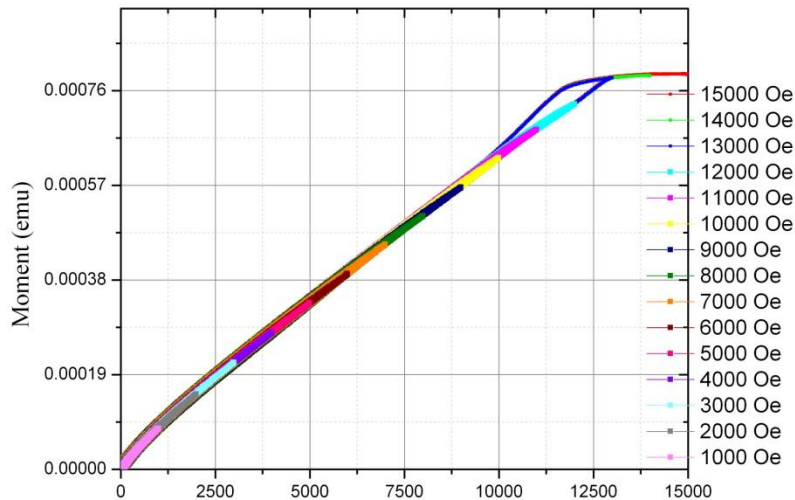


Figure 4.3. The magnetization loops of the Co/Pt thin film with Co thickness 60Å. Loops were measured in descending order, starting with the 15000 Oe and continuing down to the 500 Oe loop.

## 40Å Magnetization Loops

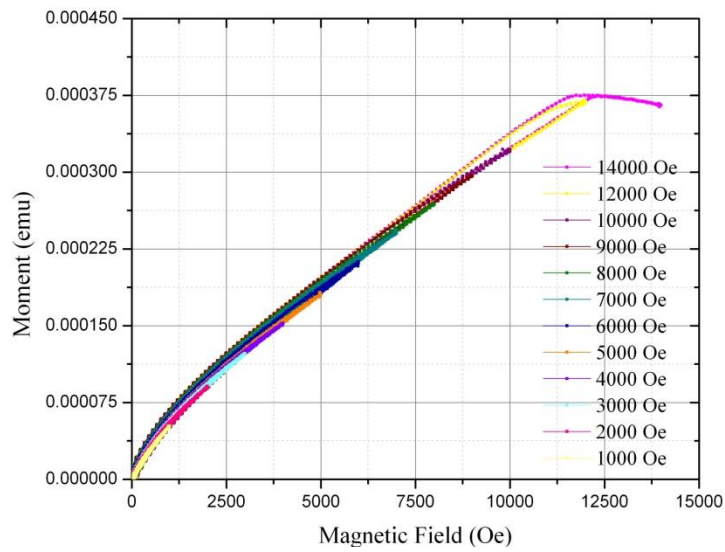


Figure 4.4. The magnetization loops of the Co/Pt thin film with Co thickness 40Å.

## 31Å Magnetization Loops

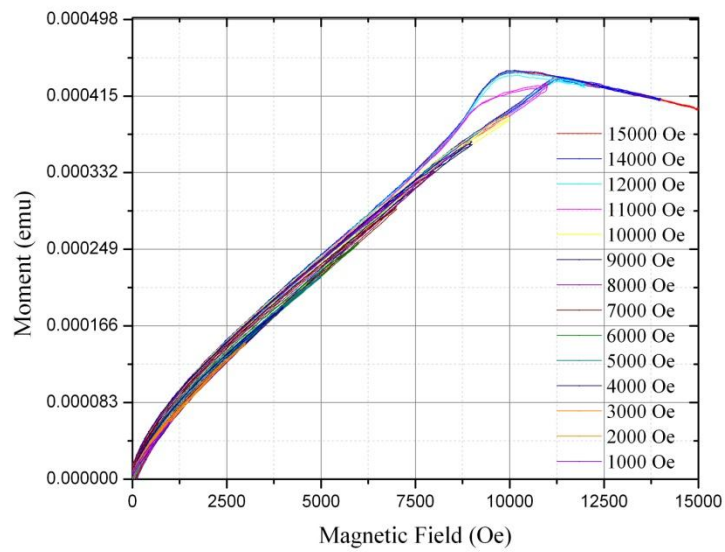


Figure 4.5. The magnetization loops of the Co/Pt thin film with Co thickness 31Å.

## 25Å Magnetization Loops

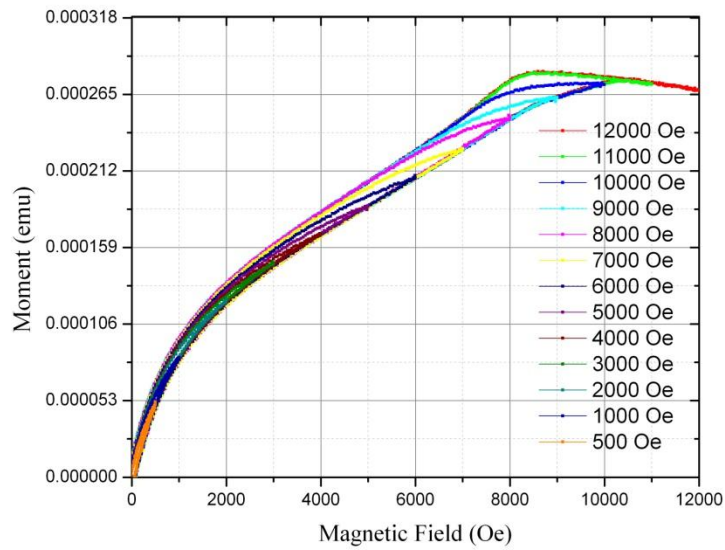


Figure 4.6. The magnetization loops of the Co/Pt thin film with Co thickness 25Å.

## 16Å Magnetization Loops

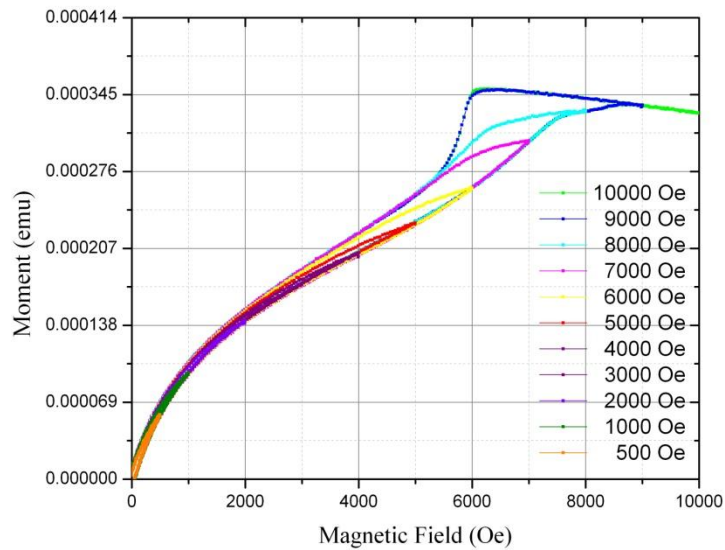


Figure 4.7. The magnetization loops of the Co/Pt thin film with Co thickness 16Å.

## 12Å Magnetization Loops

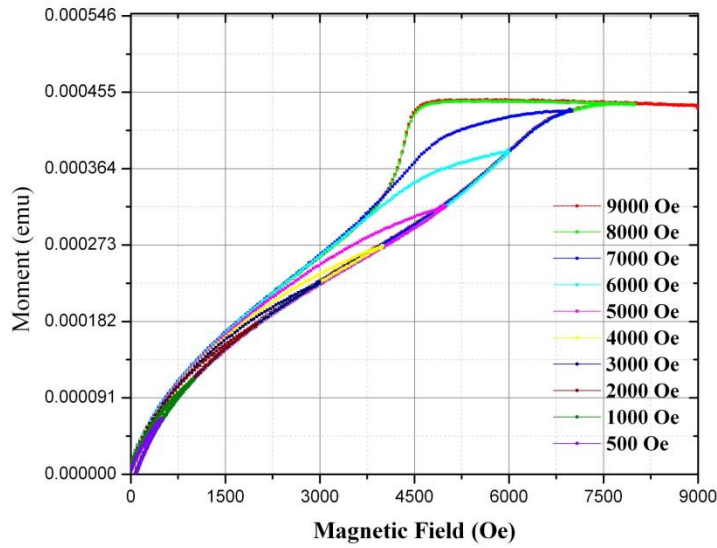


Figure 4.8. The magnetization loops of the Co/Pt thin film with Co thickness 12Å.

## 8Å Magnetization Loops

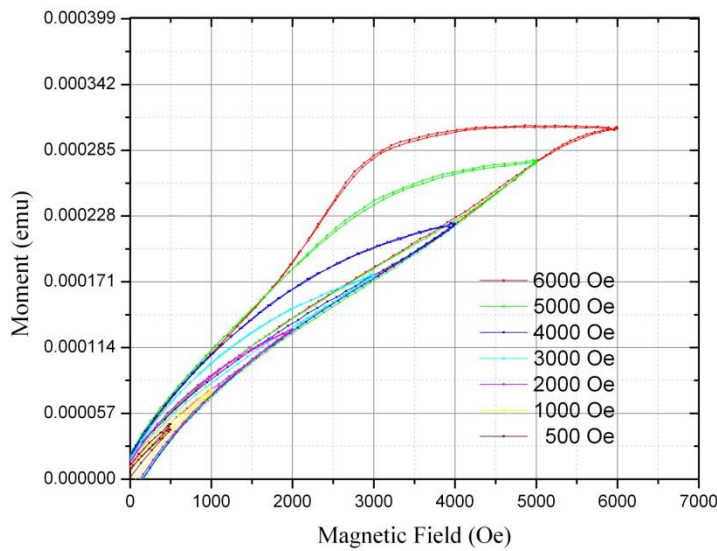


Figure 4.9. The magnetization loops of the Co/Pt thin film with Co thickness 8Å.

## 4Å Magnetization Loops

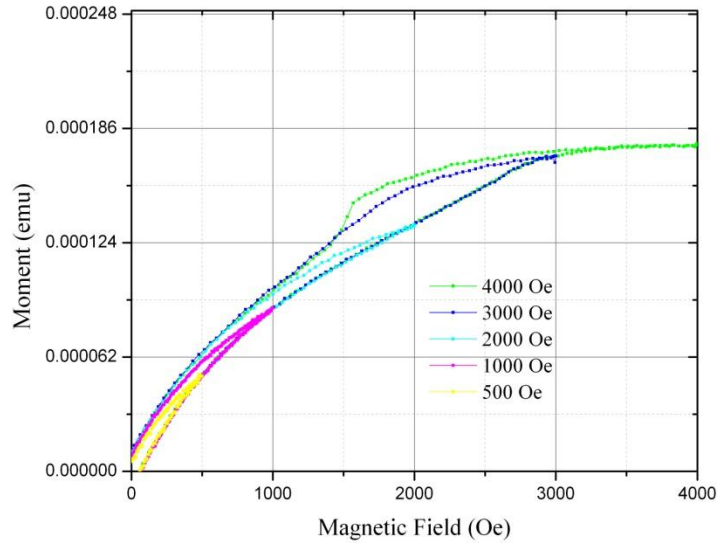


Figure 4.10. The magnetization loops of the Co/Pt thin film with Co thickness 4Å.

In an attempt to define this transition point, I determined a single transition field, denoted by  $H_t$  for each sample. I evaluated  $H_t$  by first determining a minor loop value that I could for sure say was closed, and a minor loop value that I could for sure say was open. I then took the average of these two points to determine  $H_t$ . The degree of uncertainty in  $H_t$  is shown by the error bars. Figure 4.11 a. compares  $H_s$ ,  $H_n$ , and  $H_t$  as a function of  $t_{Co}$ .  $H_t$  appears to be very similar to  $H_n$ .

Figure 4.11 b. shows  $H_t / H_s$  denoted in blue, and  $H_t / H_n$  denoted in red. The black line is the average value of  $H_t / H_n$ . The graph indicates that  $H_t \approx H_n$  within experimental error. With respect to  $H_s$  one can see that the thinner the sample is the farther  $H_t$  is from  $H_s$ .

## Comparison of $H_t$ with $H_s$ and $H_n$

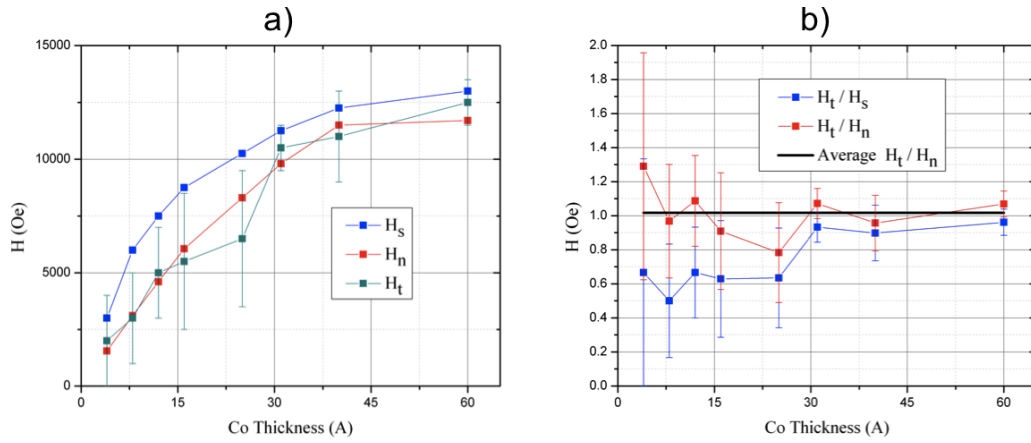


Figure 4.11. a) Shows a plot of  $H_t$ ,  $H_s$  and  $H_n$  as a function of Co thickness. b) shows  $H_t/H_s$  and  $H_t/H_n$  as a function of Co thickness.

### 4.3 Summary

There are three important phenomena observed through these magnetization loops. First  $H_s$  occurs at higher field values for larger thicknesses of Co. It also appears that  $H_s$  converges towards a maximum beyond which  $H_s$  will be independent of  $t_{Co}$ .

Second, there is a transition field,  $H_t$ , between reversible and irreversible regions of the magnetization loop. This transition is sharper for thicker samples, and more gradual for thinner samples.

Third, it appears that  $H_t$  is close to  $H_n$ .

# Chapter 5

## In-Situ MFM on 8Å Sample

In order to understand the connection between the microscopic behavior of the magnetic domains and the macroscopic behavior of the magnetization loop, I performed MFM in the presence of an in-situ magnetic field on the Co/Pt thin film with  $t_{\text{Co}}=8\text{\AA}$ .

### 5.1 Major loop in-situ MFM images

Figure 5.1 shows the MFM images corresponding to the second half of the ascending branch, from  $H=0$ , or remanence, to  $H_s$ , and the first half of the descending branch of a magnetization loop, from  $H_s$ , through  $H_n$  back to  $H=0$ . The measurement was taken in this order because of the use of permanent magnets in the In-situ MFM setup. When using permanent magnets, it is impossible to apply both a positive and a negative field in the same measurement, therefore we must start the measurement at remanence.

At remanence, long stripe domains, with magnetization pointing alternately into and out of the film plane, characterize the remnant domain morphology. As a magnetic field is applied, the aligned domains increase in size at the expense of the opposite domains. They do so while maintaining the same overall domain morphology. As the field is increased, the opposite *stripes* fragment and shrink along their length forming bubble domains.

## 8Å In-situ MFM Magnetization Loop

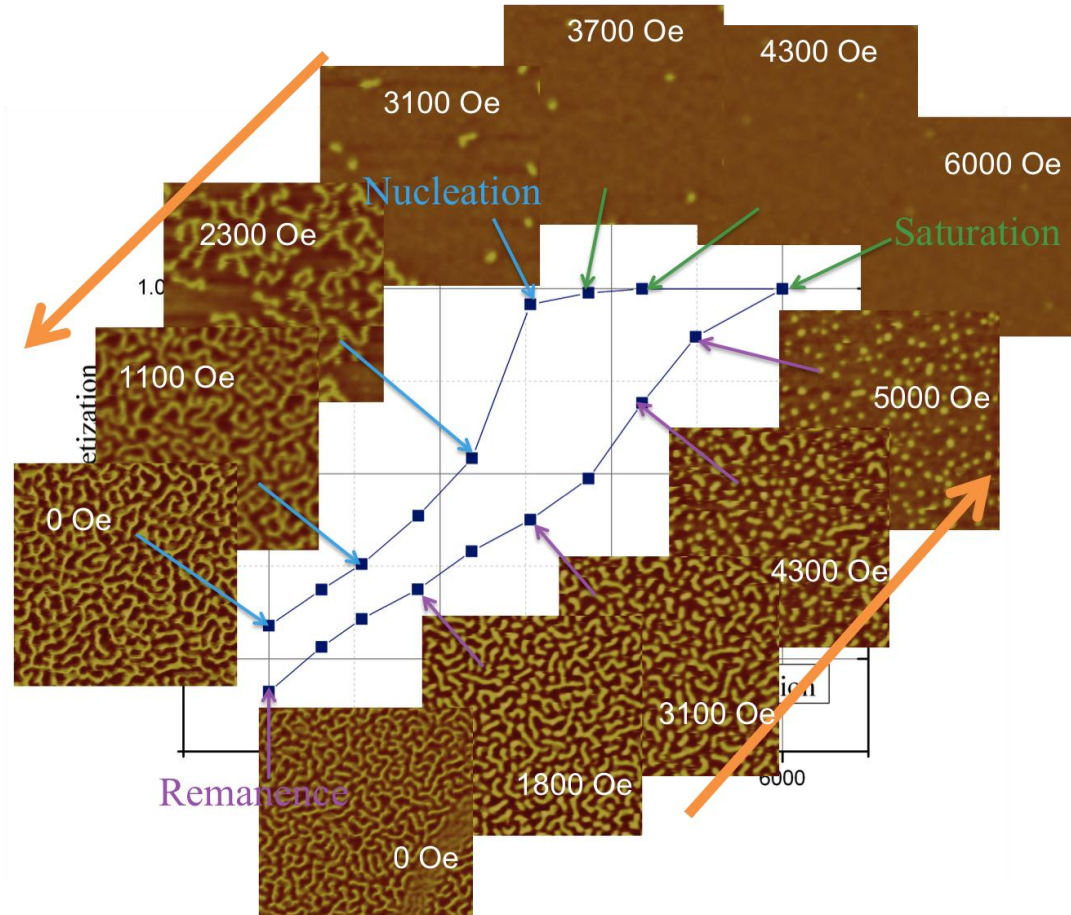


Figure 5.1. Evolution of the domain morphology of the sample with 8Å Co thickness as an external magnetic field is applied. Bottom branch is the ascending branch; top branch is the descending branch.

As the field is further increased, the bubble domains shrink to a critical diameter and then collapse.  $H_s$  occurs when all the domains have collapsed. Along the descending branch of the loop, a few domains will nucleate, and at  $H_n$  these domains will propagate to fill the sample, forming a maze pattern.

## 5.2 In-situ MFM quantitative analysis

### 5.2.1 Magnetization loop reconstruction

A quantitative analysis of the MFM images using the MIA technique, described in Chapter 3, allowed the reconstruction of the hysteresis loop seen in figure 5.2. The

reconstruction is compared with the VSM magnetization loop. The reconstructed loop matches well at remanence,  $H_s$  and  $H_n$ , but the intermediate points on both the ascending and descending branches sag. This is primarily due to an artifact in the MFM software that automatically adjusts the images to obtain the optimum contrast. This is especially a problem when the domain morphology is in a stripe state. As the opposite domains decrease in width, and the aligned domains increases in width, the program tries to maintain an equal number of pixels in either direction. This makes magnetization loop reconstruction difficult.

## Magnetization Loop Reconstruction

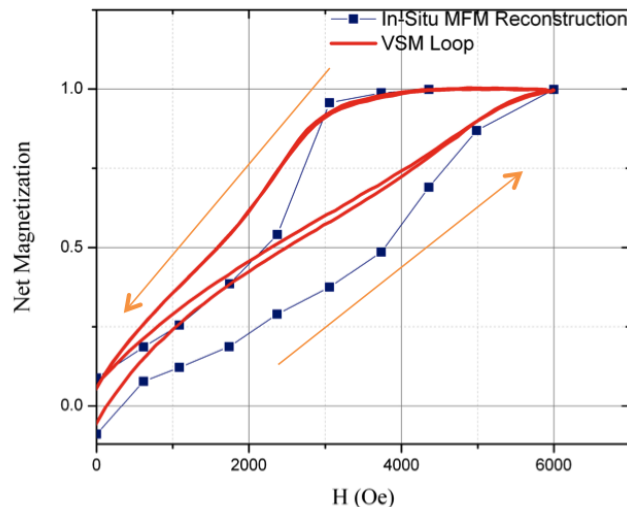


Figure 5.2. Blue curve is the reconstruction of magnetization loop from In-situ MFM images. The red curve is the VSM loop for the same sample. Yellow arrows represent the direction the loop was applied.

Despite the errors in the reconstructed magnetization loop, the qualitative behavior of the loop is in close agreement with the VSM data. This provides some assurance that the observed evolution of the domain pattern that was observed is indeed an accurate description of the microscopic origin of the macroscopic magnetization behavior.

## 5.2.2 Number of domains

As part of the quantitative analysis, I counted the number of domains in each MFM image as seen in figure 5.3. There are several important observations. First, the domains on the ascending branch immediately start to increase in number. This means that some domains immediately start to break up into smaller domains.

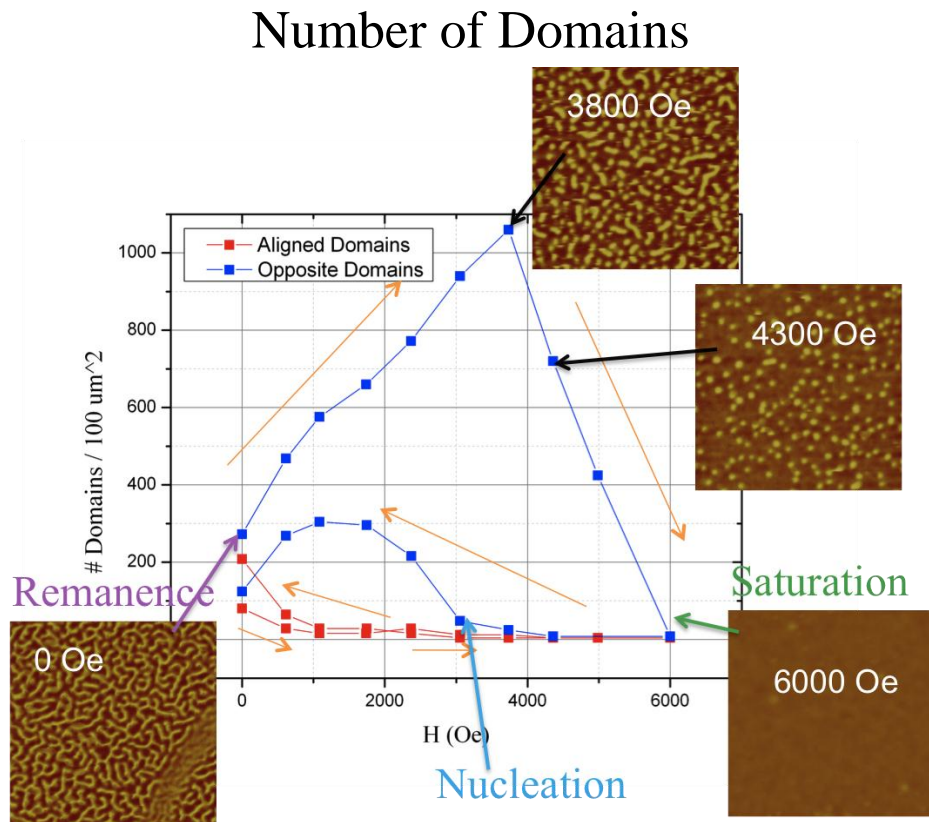


Figure 5.3. Number of domains as a function of applied field. Number of domains were determined from MFM images along a magnetization loop. Blue represents the domains pointing opposite the field. Red represents domains aligned with the field.

Second, the number of domains reaches a maximum at  $H \approx 3800 \text{ Oe}$ . At this peak, the majority of the opposite domains have contracted down to bubbles. I shall denote the field value where this peak occurs as  $H_p$ . Third, beyond  $H_p$  the bubble domains quickly collapse after reaching a critical minimum size. (See Bran [10] for a detailed description

of this critical minimum domain diameter). Fourth, on the descending branch of the magnetization loop, when the field is decreased below a certain field a few domains nucleate. This can be seen in the points just above  $H_n$ . It appears that the field value at which they begin to nucleate is close to  $H_p$ . Fifth and lastly, below  $H_n$  there is a rapid increase in the number of domains as more domains nucleate followed by a decrease as the domains join together to form the final maze pattern at remanence. This behavior indicate the formation of a domain pattern.

### 5.3 Minor loop

In section 5.2.2 I found that there is an increase in the number of domains as a magnetic field is applied on the ascending branch of a magnetization loop. It is important to the understanding of Chapter 6 to know what happens to the number of domains in the final remnant state if I were to reverse the field on or near  $H_p$ . This section shows a minor loop that went to 4000 Oe, just passing  $H_p$ .

Figure 5.4 shows the set of MFM images taken along the ascending and descending branches of this minor magnetization loop. The important thing to note is that I reversed the field after reaching a bubbles state at  $H= 4000$  Oe. In this loop, I did not have images at remanence, but the 700 Oe images are close enough to remanence to give a qualitative representation of the domain pattern visible at remanence. A visual comparison to the two 700 Oe images shows that the image on the descending branch is significantly more bubbly than the conjugate point on the ascending branch.

## In-situ MFM Minor Magnetization Loop

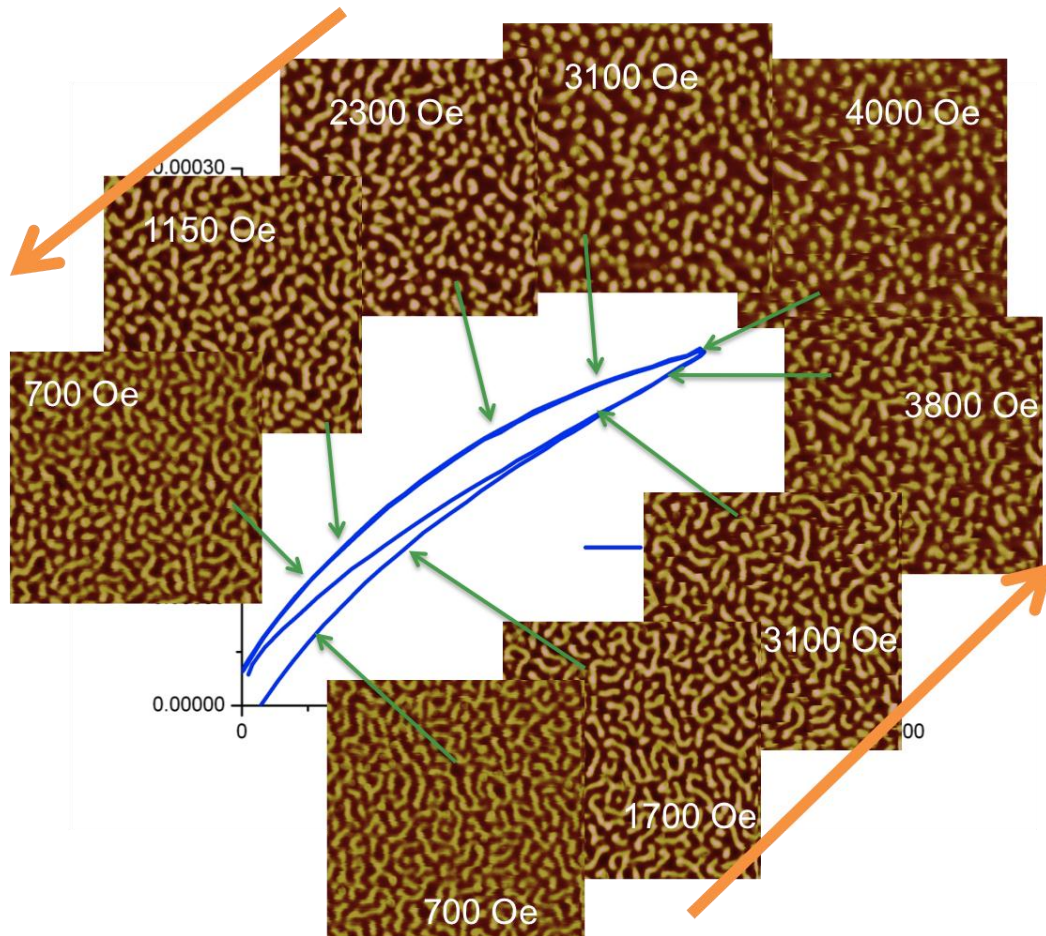


Figure 5.4. In-situ MFM of minor loop on  $8\text{\AA}$ . The field was reversed when the morphology had reached a maximum number of domains.

This result can be confirmed after counting the number of domains in each image. The number of domains for each image can be seen in figure 5.5. The 700 Oe image on the descending branch has roughly 180 more domains per  $100\ \mu\text{m}^2$  than the 700 Oe image on ascending branch.

## Minor Loop Number of Domains

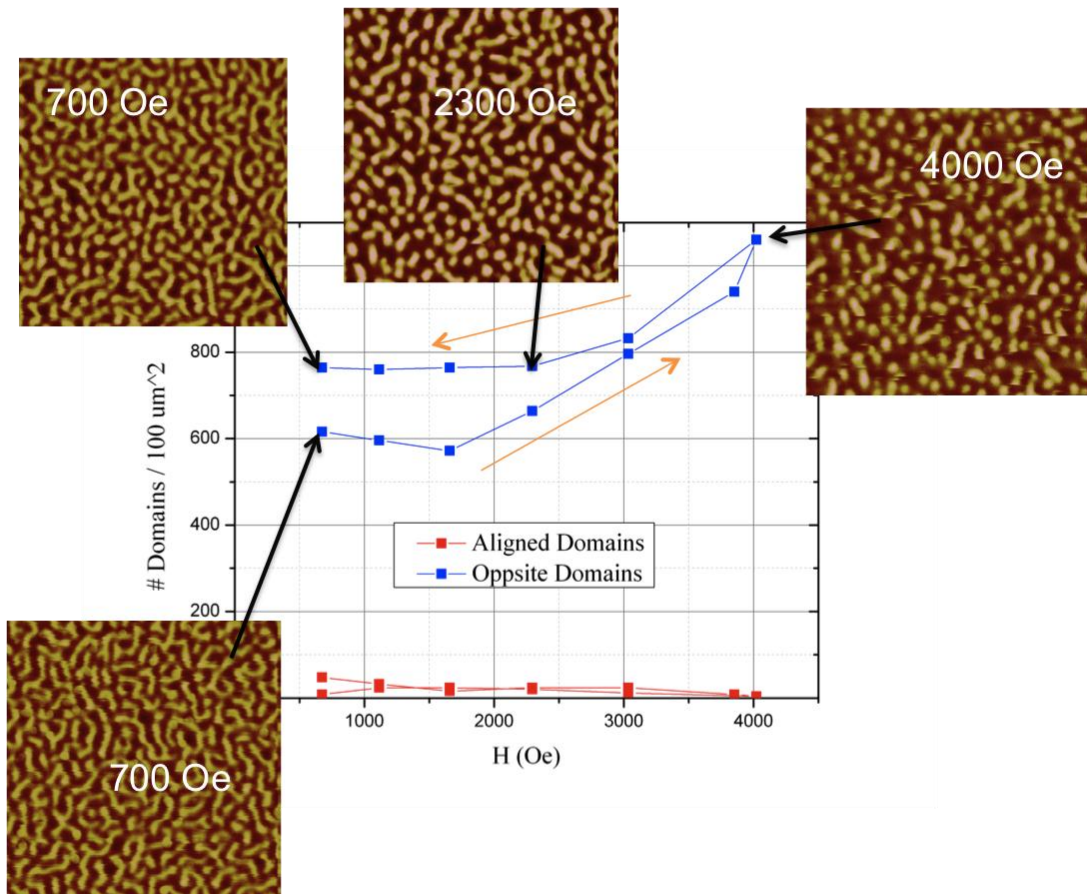


Figure 5.5. Number of domains for an In-situ MFM minor loop on the  $8\text{\AA}$  sample with a magnitude of 4000 Oe. The field was reversed when the morphology had reached a bubble state

### 5.4 Summary

Along the ascending branch of a magnetization loop the long stripe domains observed in the initial remnant domain morphology fragment and contract down to bubbles. The bubbles then shrink in diameter until reaching a minimum size and collapsing. This process causes an initial increase in the number of domains. A peak is observed in the number of the domains before the bubble domains start collapsing. Saturation is reached when all of the domains have collapsed.

When I compare the number of domains observed in a major and minor loop as seen in figure 5.3 and figure 5.5 one can see a difference in the respective number of domains before and after the loop. This corresponds to a difference in the remnant domain morphology after a major loop, and after a minor loop. In the major loop there are more domains in the remnant morphology before the loop than after the loop, but in a minor loop that stops near  $H_p$ , there is are more domains after the loop than before it. This means that the number of domains in the remnant domain morphology is tied to the maximum value of the previously applied magnetization loop.

# Chapter 6

## Remanence MFM Study

### 6.1 Remnant domain morphologies in 8Å sample

In the chapter 5 I found that the remnant domain morphology is directly connected to the magnitude of the major or minor loop applied. I will hereafter refer to the maximum value of the applied magnetization loop as  $H_L$ . In this chapter I present a study where I systematically applied major and minor magnetization loops to see the effect of different magnetization loops on remnant domain morphology.

### Experimental Process

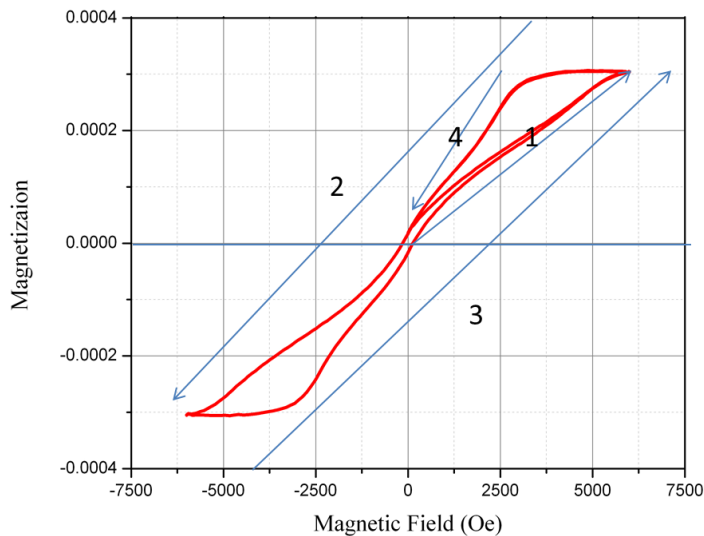


Figure 6.1. Magnetization loops were applied by first starting at remanence and increasing to a positive field value  $H_L$ : arrow 1. Then decreasing the field from  $H_L$  to  $-H_L$ : arrow 2. Increasing the field from  $-H_L$  to  $H_L$ : arrow 3. And finally decreasing the field from  $H_L$  to remanence: arrow 4. MFM images were then taken at remanence. The field value  $H_L$  was different for each loop applied.

Each magnetization loop started with field at  $H=0$ , increased the field to  $H_L$ , decreased it to  $-H_L$ , again increased it to  $H_L$ , and finally returned to remanence,  $H=0$ , as seen in figure 6.1. After each loop an MFM image was taken to observe the remnant domain morphology. Finally the number of domains in each MFM image was calculated using the MIA technique.

For ease in interpreting the data I will first present the results from the  $8\text{\AA}$  sample used for the In-situ MFM study in chapter 5.

Figure 6.2 a. shows the MFM images taken with the maximum value of its corresponding magnetization loop  $H_L$ .  $H_L$  was different for each magnetization loop applied. Visually is difficult to see any difference between the remnant domain morphologies, but when one looks at the number of domains corresponding to each image as seen in figure 6.2 b. It is clear that there is a large difference in the maximum number of domains after the different minor loops.

In figure 6.2b there are three distinct regions. Region 1) corresponding to major loops  $H_L > H_s$ . This region has a domain morphology that is closest to an equal number of opposite and aligned domains. Region 2, or the peak, occurs for  $H_L$  that is just under  $H_s$ . Region 3) occurs after  $H_L$  60% or less than that of  $H_s$ . All of these minor loops produce a similar number of domains. This number however, is greater than after the major loops seen in region 1.

In the in-situ domain morphologies there was also a peak in the number of domains (see figure 5.3). This peak does not however correspond with the peak, denoted as  $H_p^L$ , observed in the remnant domain morphology seen in figure 6.2., meaning  $H_p \neq H_p^L$ .

a)  $8\text{\AA}$  Remnant MFM Images

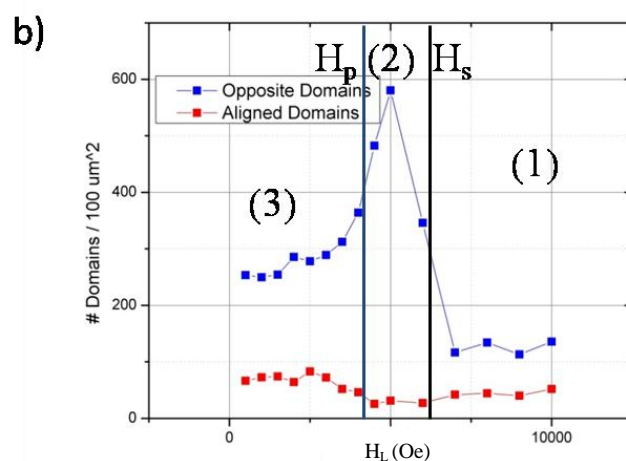
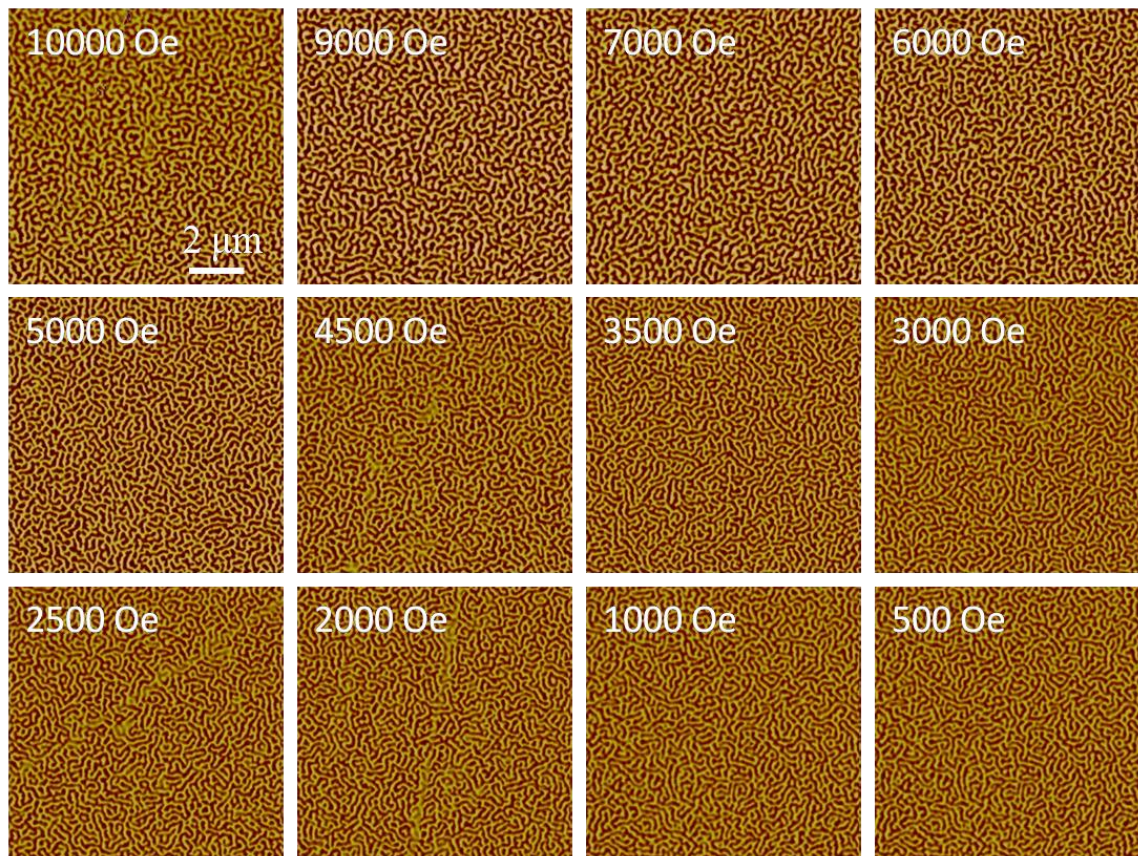


Figure 6.2. a) Remnant MFM images for  $8\text{\AA}$  sample. Images were taken after applying a minor magnetization loop with the corresponding value referring to the minor loop magnitude. Images are  $10\mu\text{m} \times 10\mu\text{m}$ . b) Number of domains corresponding to MFM images as a function of minor loop maximum field value. The black line represents the  $H_s$ . The dark blue line represents  $H_p$ . There are three distinct regions: (1) after the peak, (2) the peak, and (3) before the peak.

$H_p$  actually corresponds with the base of the peak observed in figure 6.2, forming the dividing point between regions 2 and 3. This may possibly be due to a combination of the effects of splitting and fragmentation, and nucleation of domains. After  $H_p$ , the domains start collapsing. Once domains start collapsing, there is the possibility for additional domains to start nucleating if the field is reversed. Thus in minor loops with  $H_L$  that passes  $H_p$ , but does not draw too close to  $H_s$ , there is a maximum in the number of domains seen at remanence. This could be because there are still a large number of domains that have not collapsed, but there are also a significant number of domains that nucleate as the field is returned to remanence.

Another important point to note is the location of saturation as seen on the magnetization loops in comparison with the point where the peak ends in region 1. Saturation occurs at 6000 Oe, and the end of the peak occurs at 7000 Oe. It can be thought that the end of the peak should correspond with saturation. This discrepancy can be explained by the observation of Davies, et al. [9]. They observed that after apparent saturation on the magnetization loop there are still a few residual bubbles domains that have contracted in size but not collapsed. If the field is not increased to the point where these residual domains collapse they provide sites for nucleation and affect the domain morphology all along the descending branch of the magnetization loop. They thus make the argument that true saturation occurs after the saturation observed in a magnetization loop. These residual domains could easily cause a difference in the number of domains in the remnant domain morphology observed between the 6000 Oe and 7000 Oe major loops.

## 6.2 Remnant domain morphologies across thickness

Figures 6.3-6.10 show the results of the same minor loops study presented in section 6.1 for all 8 of our samples. The results of the 8Å sample are also presented so that they can be seen in order, from the thickest 60Å sample to the thinnest 4Å sample. All of the samples show a similar behavior with the 3 regions presented in section 6.1: 1) after the peak, 2) the peak, 3) before the peak. There are however two important differences across the samples.

First at  $H_p^L$  there is a stark difference in the domain morphology between the thinner samples  $t_{Co} \leq 16\text{\AA}$  and the thicker samples  $t_{Co} \geq 25\text{\AA}$ . Although there is a difference in the number of domains  $H_p^L$ , and regions 1 and 3, visually the domains still appear to be long stripe domains. For the thicker samples the morphology at  $H_p^L$  clearly forms a bubble pattern. This is especially pronounced for the 31Å sample. Second, in the thinner samples, region 1 has fewer domains than in region 3, but in the thicker samples region 3 has significantly fewer domains than in region 1. This will be analyzed in more detail in section 6.3.

a)  $60\text{\AA}$  Remnant MFM Images

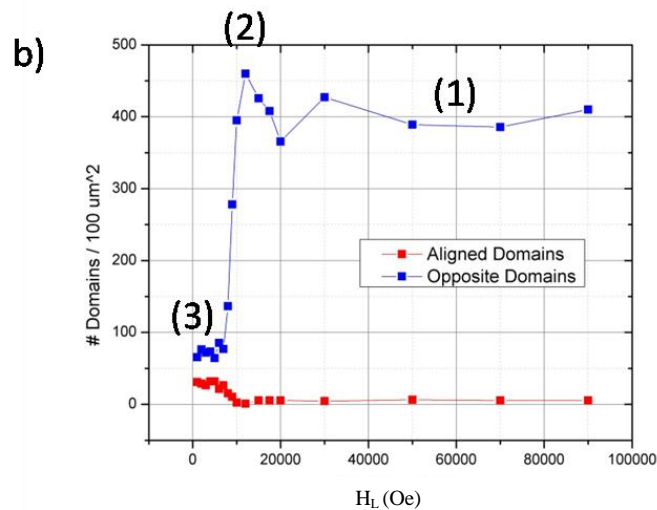
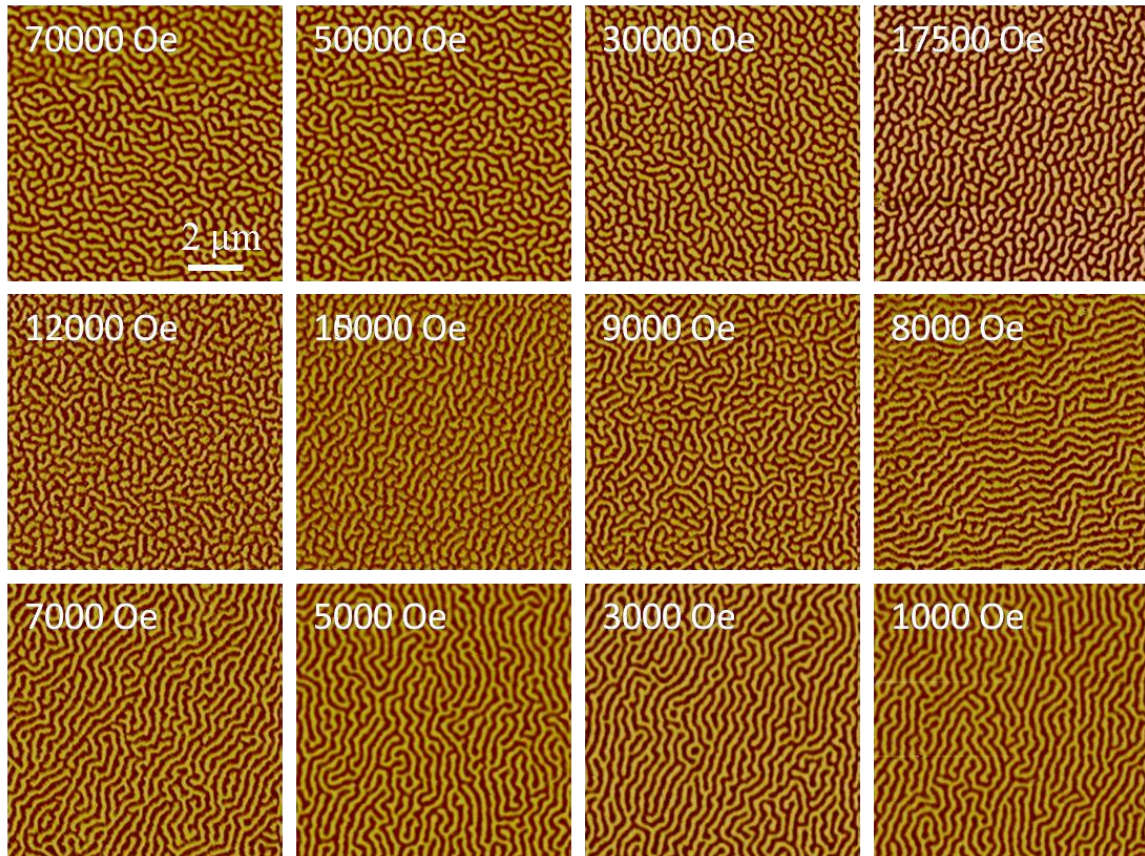


Figure 6.3. a) Remnant MFM images for  $60\text{\AA}$  sample. Images were taken after applying a minor magnetization loop with the corresponding value referring to the minor loop magnitude. Images are  $10\mu\text{m} \times 10\mu\text{m}$ . b) Number of domains corresponding to MFM images as a function of minor loop maximum field value. There are three distinct regions: (1) after the peak, (2) the peak, and (3) before the peak.

a) 40Å Remnant MFM Images

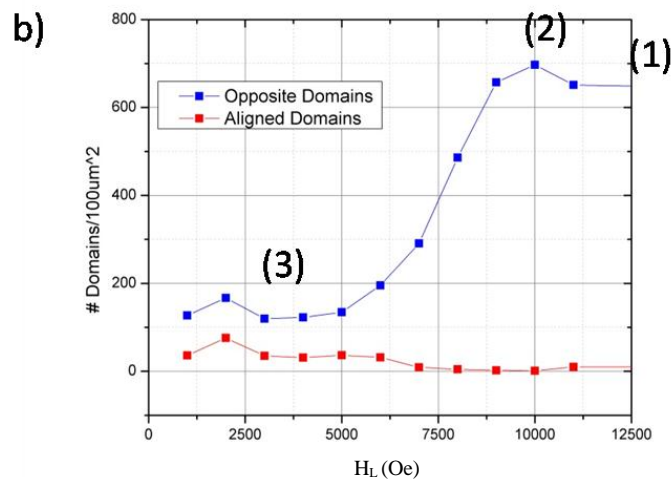
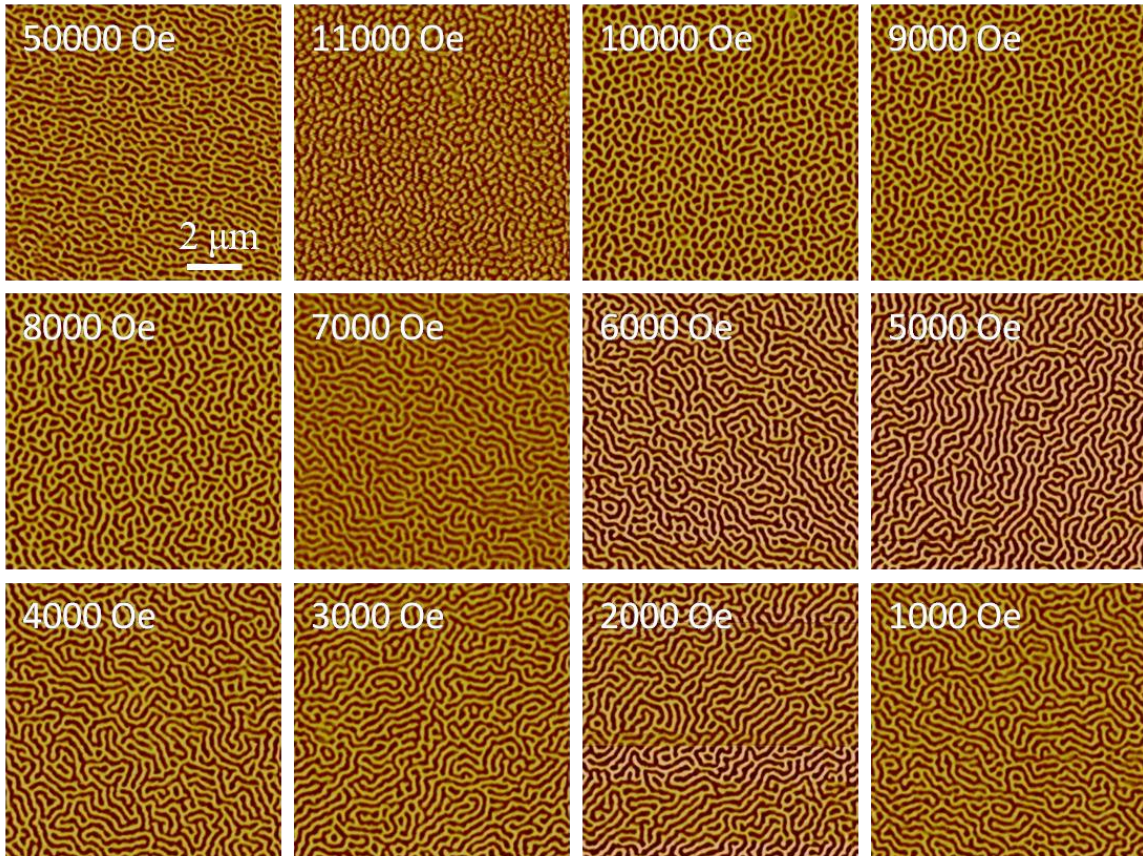


Figure 6.4. a) Remnant MFM images for 40Å sample. Images were taken after applying a minor magnetization loop with the corresponding value referring to the minor loop magnitude. Images are 10 $\mu\text{m}$  x 10 $\mu\text{m}$ . b) Number of domains corresponding to MFM images as a function of minor loop maximum field value. There are three distinct regions: (1) after the peak, (2) the peak, and (3) before the peak.

a)  $31\text{\AA}$  Remnant MFM Images

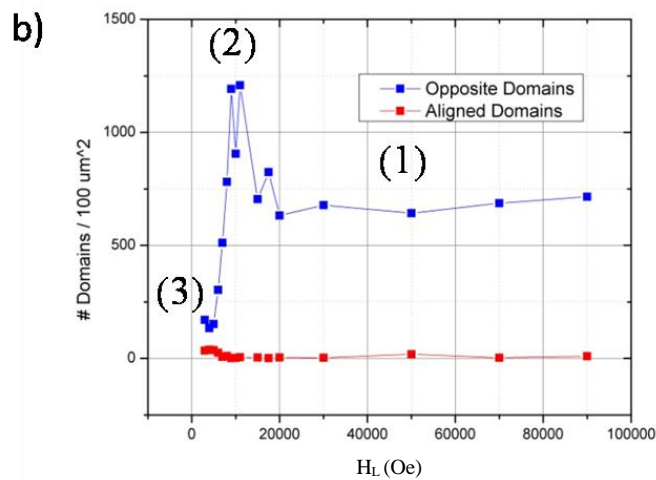
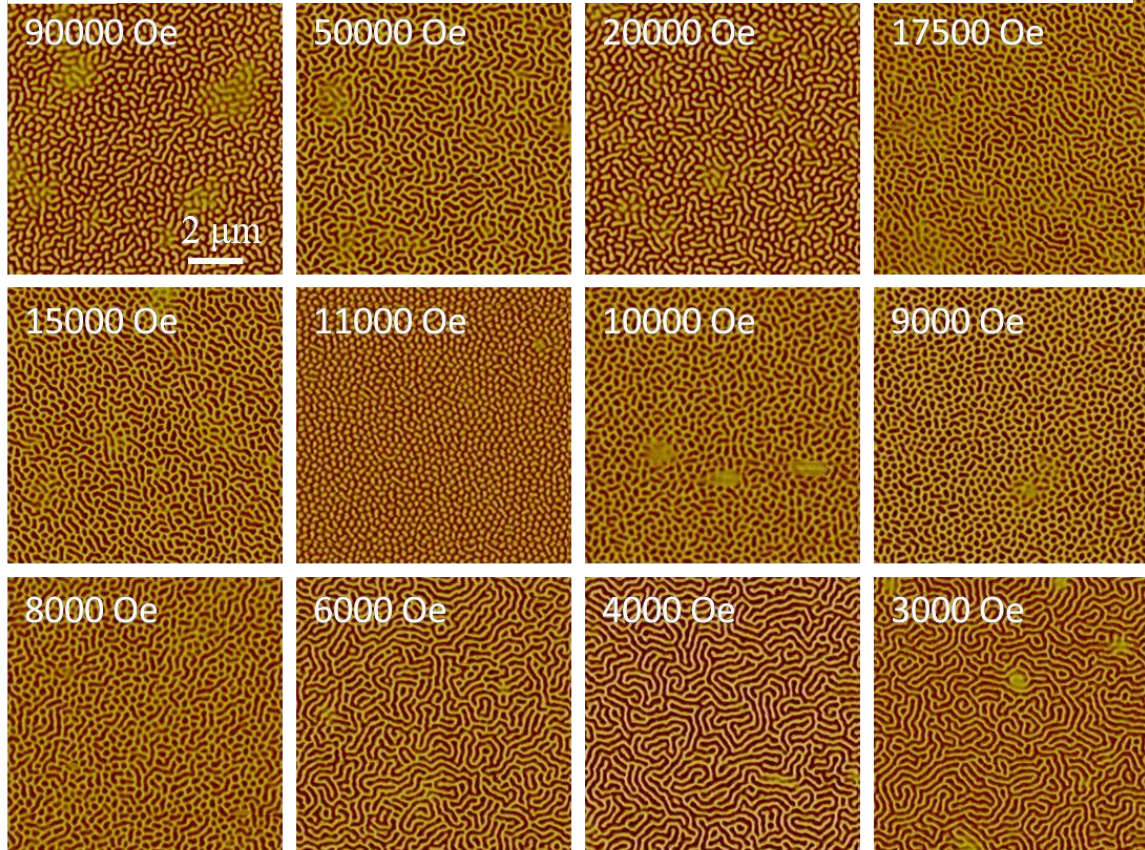


Figure 6.5. a) Remnant MFM images for  $31\text{\AA}$  sample. Images were taken after applying a minor magnetization loop with the corresponding value referring to the minor loop magnitude. Images are  $10\mu\text{m} \times 10\mu\text{m}$ . b) Number of domains corresponding to MFM images as a function of minor loop maximum field value. There are three distinct regions: (1) after the peak, (2) the peak, and (3) before the peak.

a)  $25\text{\AA}$  Remnant MFM Images

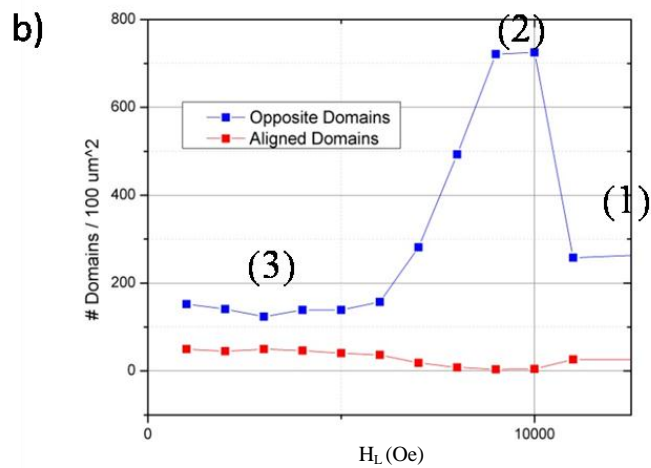
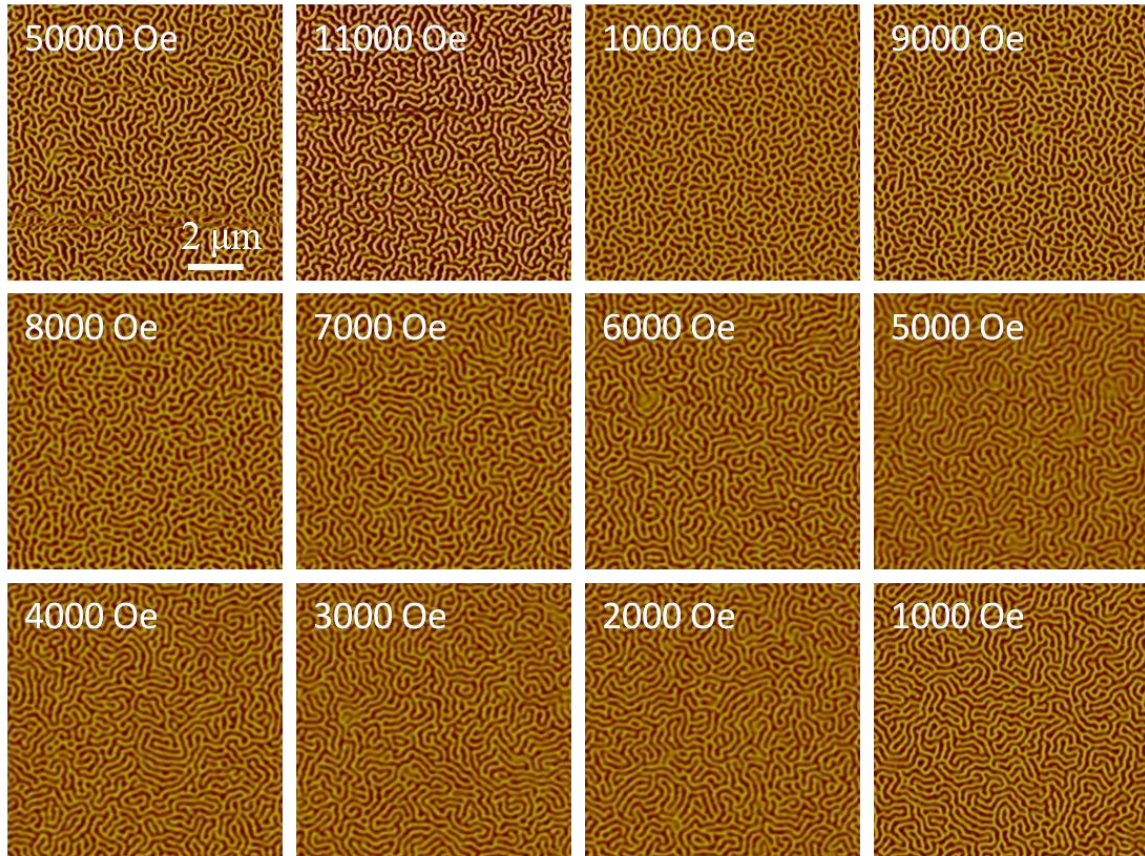


Figure 6.6. a) Remnant MFM images for  $25\text{\AA}$  sample. Images were taken after applying a minor magnetization loop with the corresponding value referring to the minor loop magnitude. Images are  $10\mu\text{m} \times 10\mu\text{m}$ . b) Number of domains corresponding to MFM images as a function of minor loop maximum field value. There are three distinct regions: (1) after the peak, (2) the peak, and (3) before the peak.

a)  $16\text{\AA}$  Remnant MFM Images

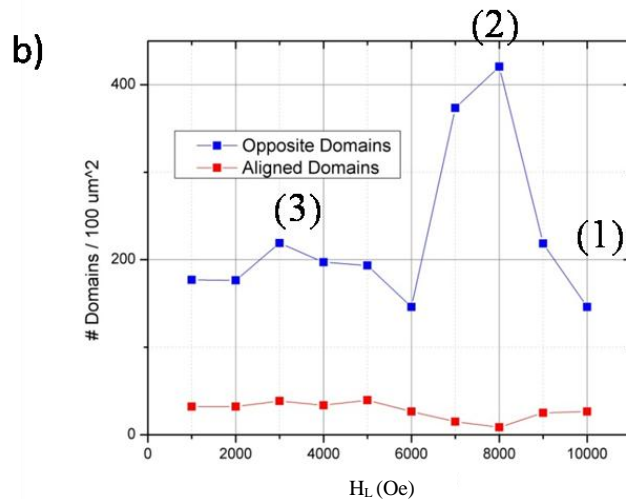
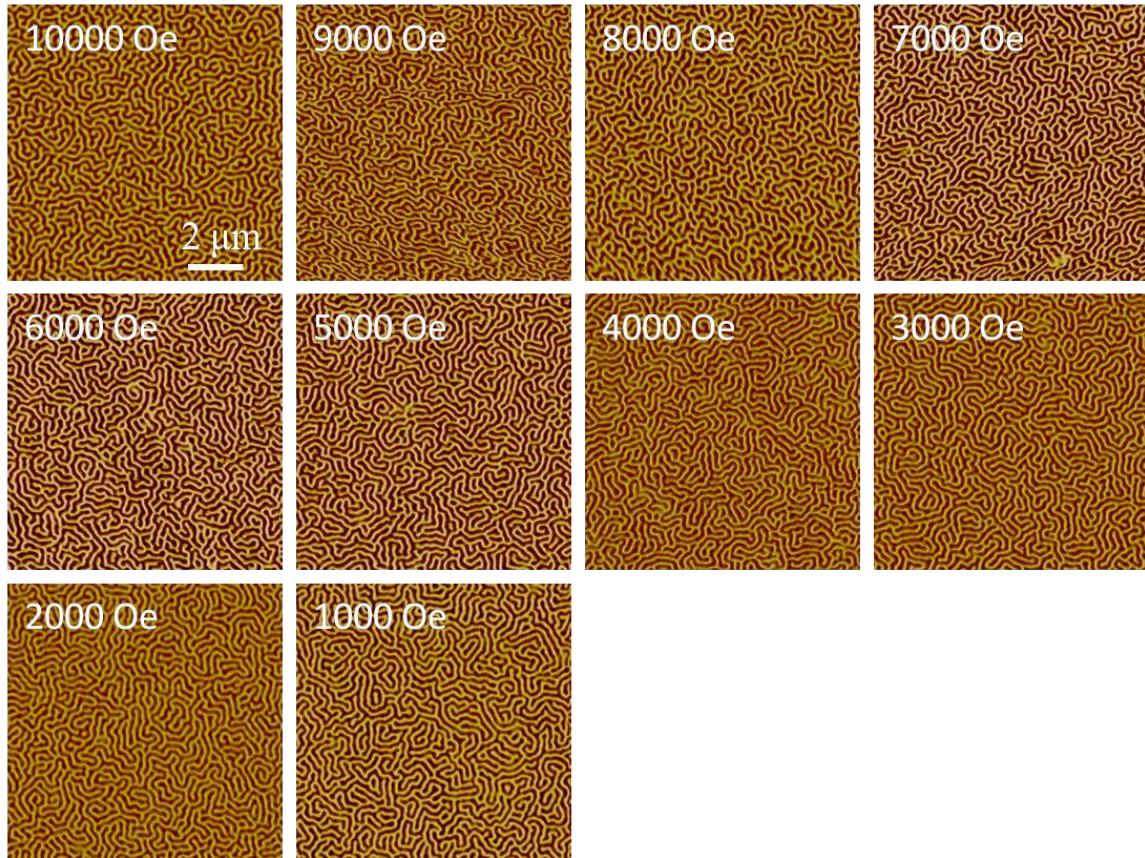


Figure 6.7. a) Remnant MFM images for 16A sample. Images were taken after applying a minor magnetization loop with the corresponding value referring to the minor loop magnitude. Images are  $10\mu\text{m} \times 10\mu\text{m}$ . b) Number of domains corresponding to MFM images as a function of minor loop maximum field value. There are three distinct regions: (1) after the peak, (2) the peak, and (3) before the peak.

a)  $12\text{\AA}$  Remnant MFM Images

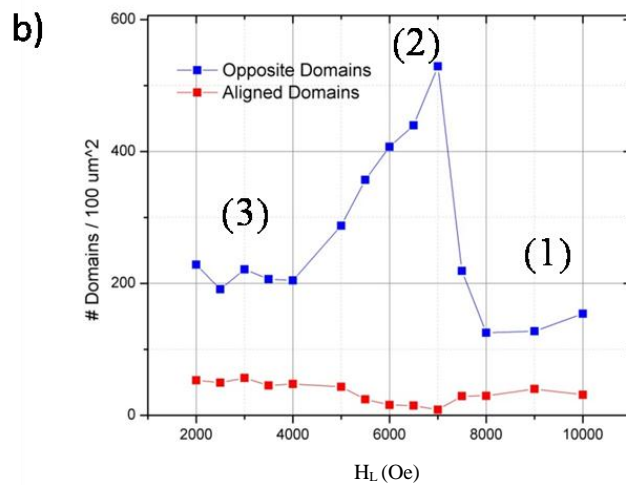
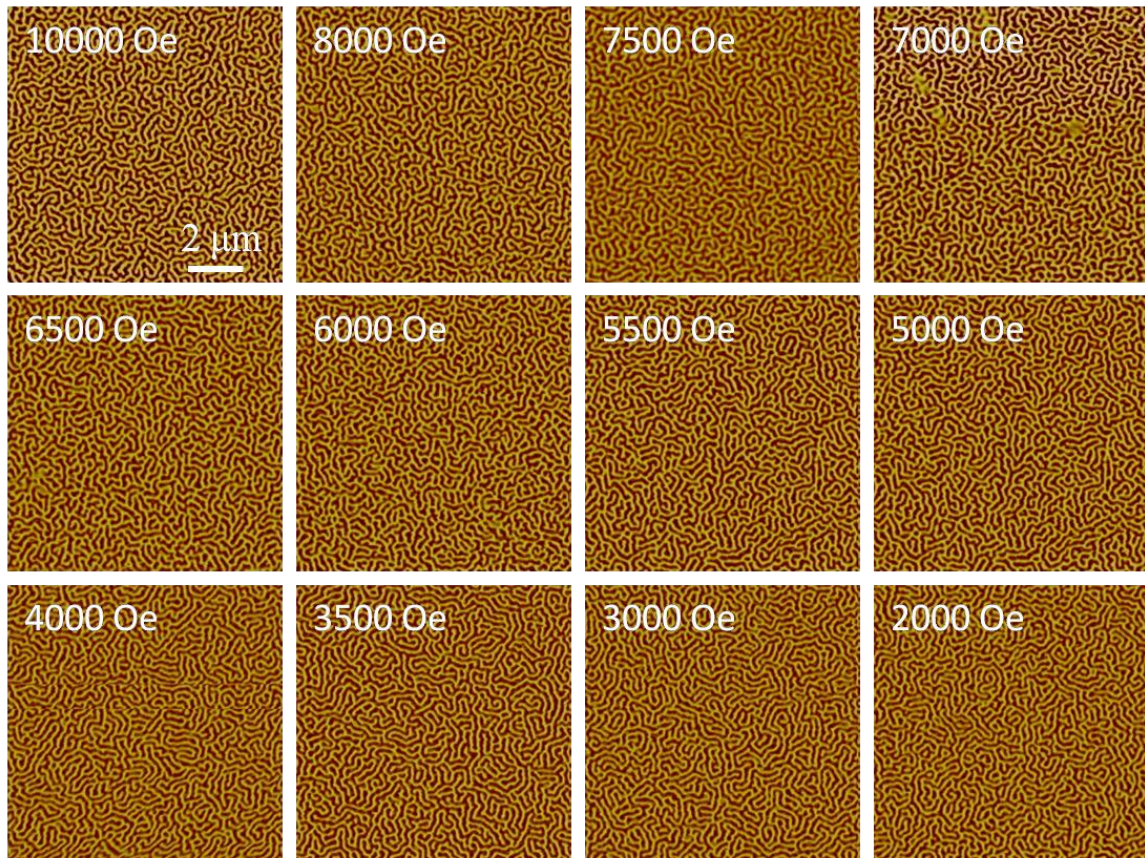


Figure 6.8. a) Remnant MFM images for  $12\text{\AA}$  sample. Images were taken after applying a minor magnetization loop with the corresponding value referring to the minor loop magnitude. Images are  $10\mu\text{m} \times 10\mu\text{m}$ . b) Number of domains corresponding to MFM images as a function of minor loop maximum field value. There are three distinct regions: (1) after the peak, (2) the peak, and (3) before the peak.

a)  $8\text{\AA}$  Remnant MFM Images

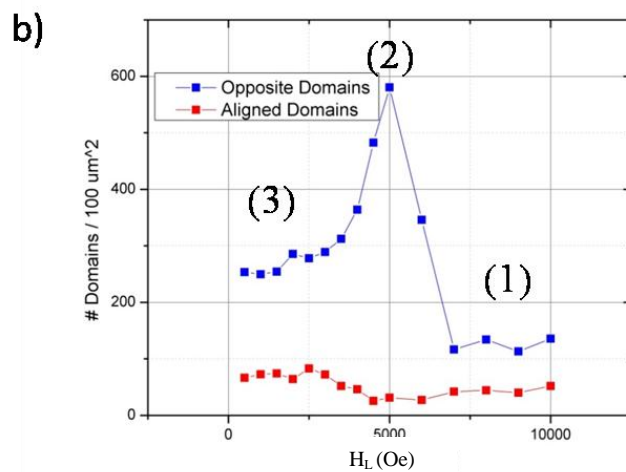
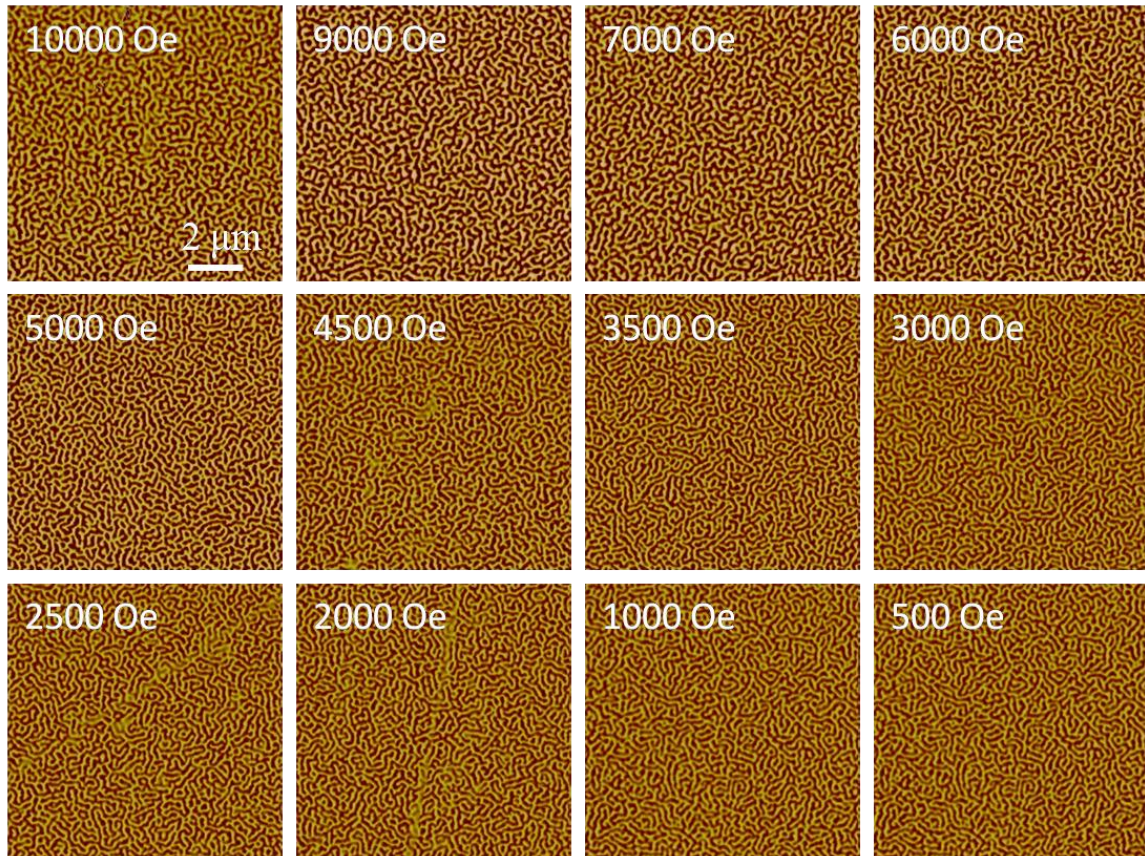


Figure 6.9. a) Remnant MFM images for 8A sample. Images were taken after applying a minor magnetization loop with the corresponding value referring to the minor loop magnitude. Images are  $10\mu\text{m} \times 10\mu\text{m}$ . b) Number of domains corresponding to MFM images as a function of minor loop maximum field value. There are three distinct regions: (1) after the peak, (2) the peak, and (3) before the peak.

a)  $4\text{\AA}$  Remnant MFM Images

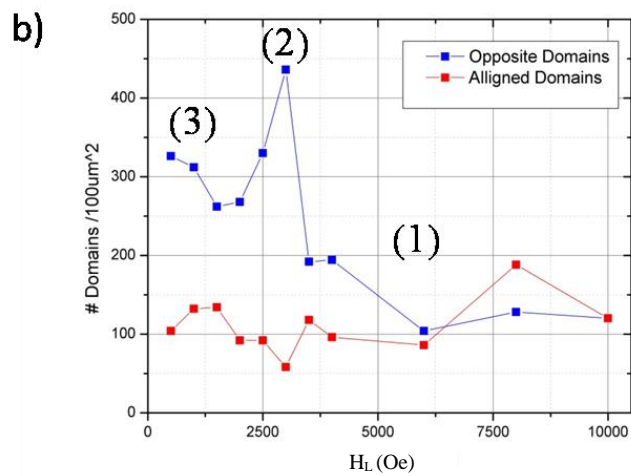
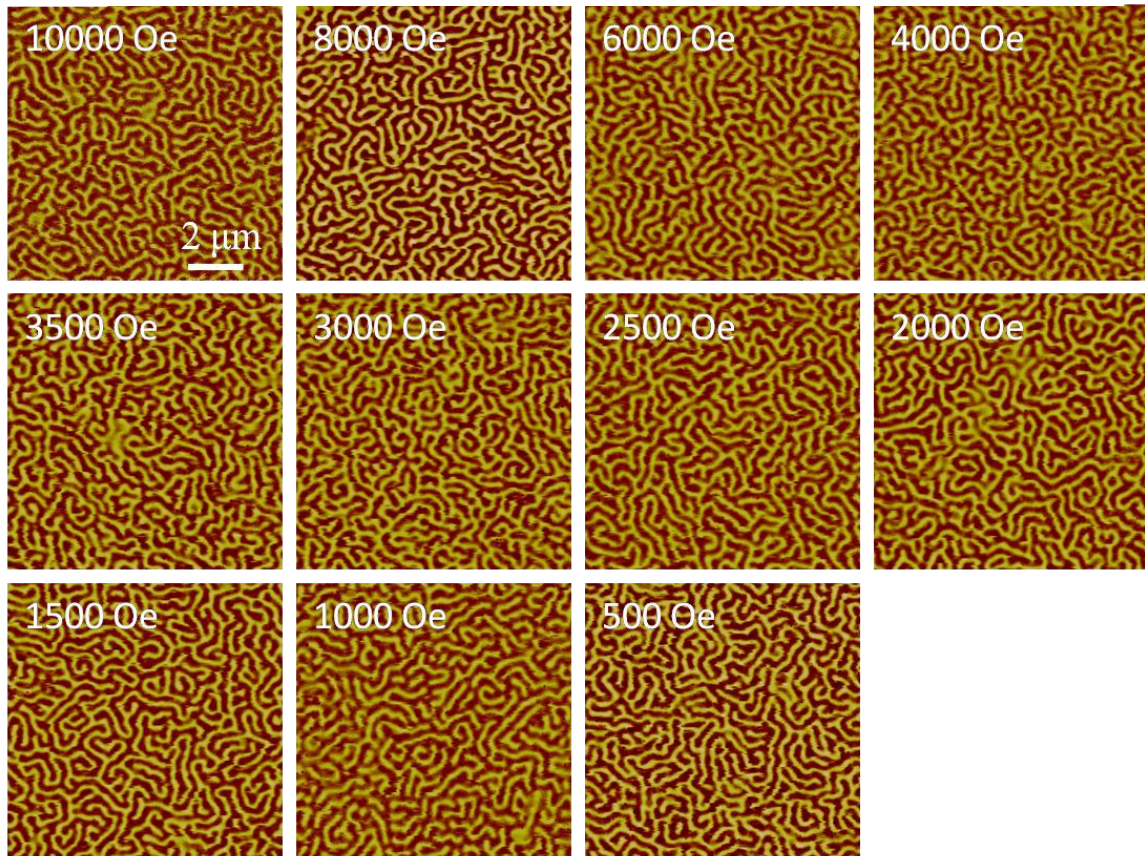


Figure 6.10. a) Remnant MFM images for  $4\text{\AA}$  sample. Images were taken after applying a minor magnetization loop with the corresponding value referring to the minor loop magnitude. Images are  $10\mu\text{m} \times 10\mu\text{m}$ . b) Number of domains corresponding to MFM images as a function of minor loop maximum field value. There are three distinct regions: (1) after the peak, (2) the peak, and (3) before the peak.

## 6.3 Analysis of remanence MFM images across thickness

### 6.3.1 Minor loop peak position vs. saturation

Figure 6.11 a. shows  $H_p^L$  as a function of  $t_{Co}$ . Qualitatively this behavior is similar to that of saturation seen in figure 4.2. Figure 6.11 b shows the peak position divided by the  $H_s$ . The black line is 90% of saturation. For all of the samples,  $H_p^L$  occurred at about 90% of  $H_s$ . Thus the peak occurs just before saturation in all of the samples except for the 4Å. In reality it probably does occur before saturation for the 4Å sample, but because our step size is 500Oe there is a large degree of uncertainty in  $H_p^L$ .

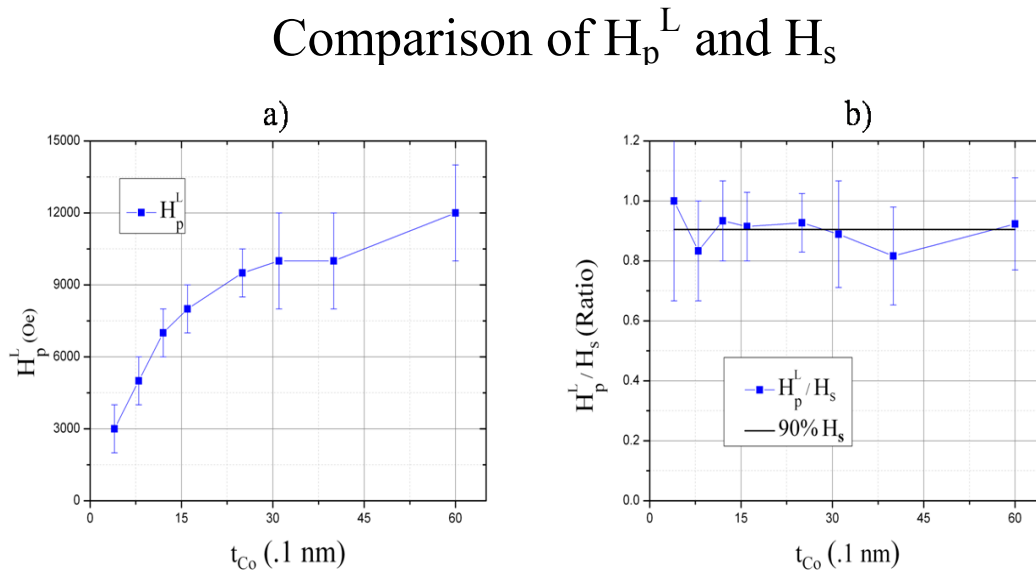


Figure 6.11. a) Shows a plot of  $H_p^L$  as a function of  $t_{Co}$ . b)  $H_p^L / H_s$  as function of  $t_{Co}$ . The black line is 90% of  $H_s$  and was drawn in for comparison purposes.

### 6.3.2 Number of domains at the peak vs. $t_{Co}$

Figure 6.12 shows the number of domains at  $H_p^L$  as a function of  $t_{Co}$ . There is a definite change in the number of domains at the peak across  $t_{Co}$ . Without a larger number of

samples it is difficult to obtain the complete picture, but it is clear that a maximum occurs in the number of domains at 31 Å.

### Number of Domains at $H_p^L$ vs. $t_{Co}$

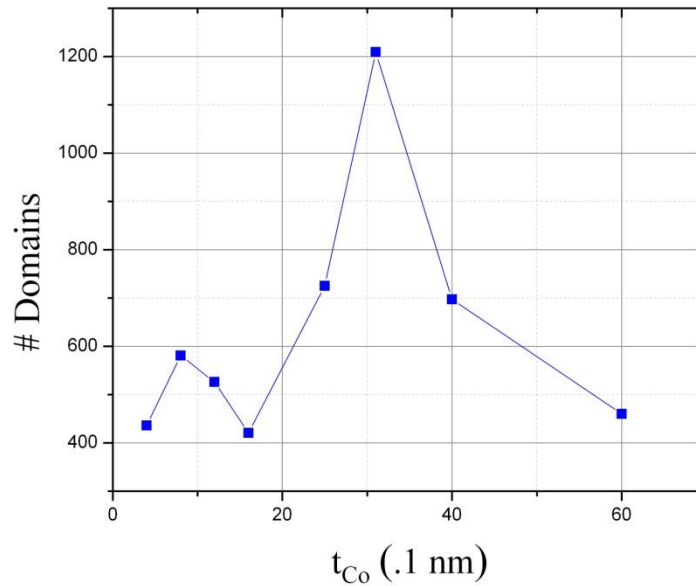


Figure 6.12. a) Shows a plot of  $H_p^L$  as a function of  $t_{Co}$ . b)  $H_p^L / H_s$  as function of  $t_{Co}$ . The black line is 90% of  $H_s$  and was drawn in for comparison purposes.

### 6.3.3 Number of domains vs. $t_{Co}$ and $H_L$

Figure 6.13. provides a summary of all the data for the number of domains vs.  $t_{Co}$  and  $H_L$ . The peak positions can be seen along the ridge marked by the black line. The maximum in the number domains across thickness and  $H_L$ , is clearly seen as the red maximum towards the center of the plot. The top half of the graph shows a clear difference in region 1, the morphology after  $H_s$ . The bottom portion of the graph shows the difference in region 3, the morphology before the peak.

## Number of Domains vs. $H_L$ and $t_{Co}$

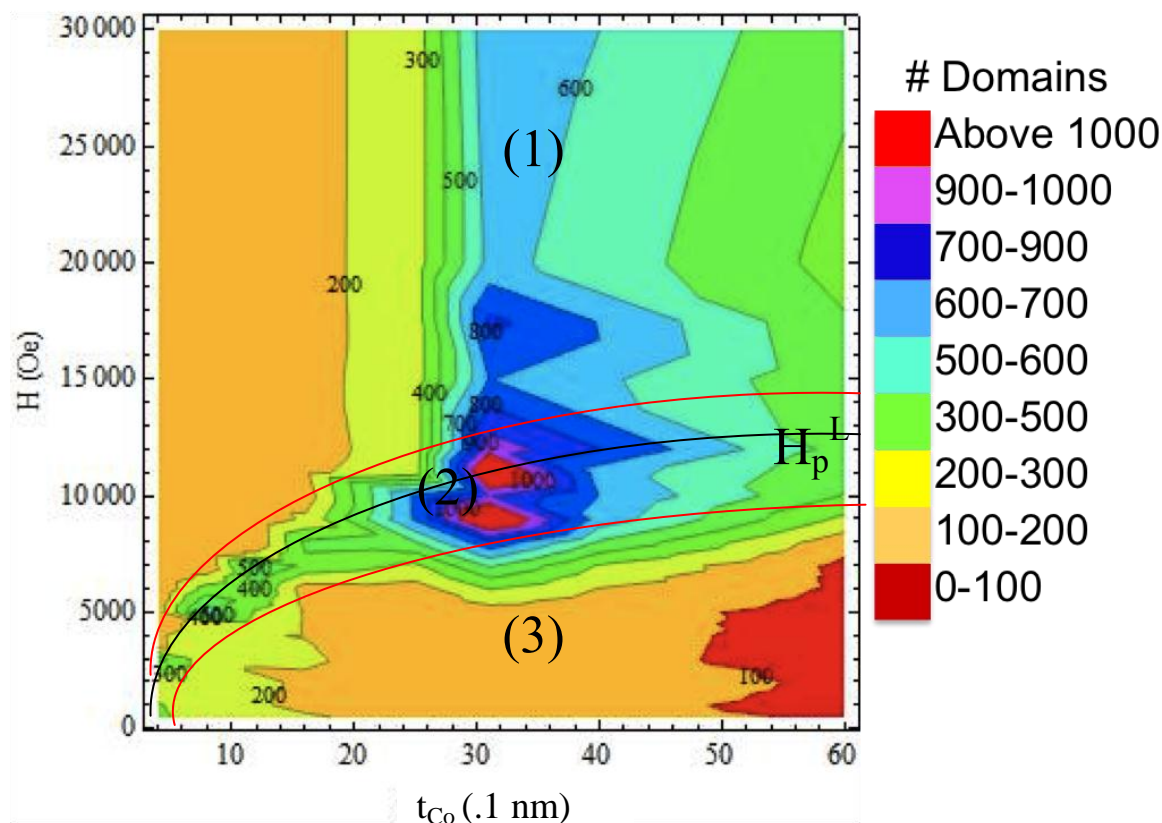


Figure 6.13. Presents a contour plot. The y-axis is  $H_L$ ; the x-axis is  $t_{Co}$ . The intensity is the number of domains for a given  $H_L$  and  $t_{Co}$ . The black line represents the position of  $H_p^L$ . The red lines roughly mark the boundaries between regions 1: after the peak, 2: the peak, and 3: before the peak.

This general difference in the behavior across thickness may be due to demagnetization fields. Just as the atoms in ferromagnetic materials have coupled spins causing them to form domains, the domains in materials are also coupled. This interacting field between neighboring domains is called the demagnetization field. The thicker  $t_{Co}$  is, the larger the demagnetization fields are. Because of these larger demagnetization fields, bubble domains become more stable. For the thinner samples, when a field is reversed after producing a bubble domain morphology as seen in the in-situ MFM images, the bubble

domains start to join back together to form stripe domains again. For the thicker samples however, the large demagnetization fields stabilize the bubble domains preventing them from joining back together. This could also explain why the thickest samples have fewer domains at the peak than the samples with middling thickness. Because of the demagnetization fields it is actually more difficult to split the stripe domains and reduce them to bubbles. If this is the case, then for the thickest samples a full bubble state is never reached.

One of the most interesting effects is what happens after the major loops. Saturation is defined as the state where all of the opposite domains have been collapsed. In the thinner films, when the field is then brought back to remanence a maze morphology is produced. When the thicker samples are saturated and then brought back to remanence they do not produce a maze configuration. On the contrary they produce a combination of short stripes and bubbles. This could also be due to the demagnetization fields. The demagnetization fields tend to support domain patterns with a larger number of domains. In the thicker samples, when domains nucleate and start to spread out to fill the sample, the larger demagnetization fields prevent the domains from completely joining together causing a mixed bubble short stripe pattern. In order to produce a maze pattern in the thicker samples minor loops with maximum values well below saturation must be applied.

# Chapter 7

## Conclusion

In summary I have used VSM, EHE, and MFM to study the effect of Co thickness on the magnetization behavior, the general field evolution of magnetic domain morphology, and the effect of Co thickness and magnetization loops on remnant domain morphologies in. The magnetization loops reveal a clear increase in the saturation and nucleation fields across thickness. They also show a clear decrease in the amount of hysteresis as Co thickness increases. In-situ MFM measurements of the field evolution of domain morphology show that initial remnant stripe domains fragment and shrink along their length forming into bubbles. The number of domains reaches a maximum in this state. As the field is further increased the bubble domains collapse. Saturation is reached when all of the domains have collapsed. When the field is reversed after reaching saturation, a few domains nucleate and then expand again forming a long stripe domain morphology. A systematic study of remnant domain morphology after magnetization loops with differing magnitude showed that when minor loops are applied there is often a large difference in the number of domains in the remnant morphology before and after the loop. In fact there is a maximum in the number of domains in the remnant domain morphology after minor loops that reach about 90% of the saturation field. This behavior is true for all of the samples, but is more pronounced for the thicker samples. The thicker samples actually tend to produce bubble patterns for larger magnetization loops. They even produce mixed bubble/stripe patterns after major magnetization loops. These results are probably due to the stronger demagnetization fields of the thicker samples.

# Bibliography

- [1] D. J. Griffiths, Introduction to Quantum Mechanics, 2nd ed. (Prentice-Hall, Inc., New Jersey, 1995).
- [2] D. J. Griffiths, Introduction to Electrodynamics, 3rd ed. (Prentice-Hall Inc., New Jersey, 1999).
- [3] A. W. Rushforth, P. C. Main, B. L. Gallagher, C. H. Marrows, B. J. Hickey, E. D. Dahlberg, and P. Eames, J. Appl. Phys. **89**, 7534 (2001).
- [4] M. Labrune and L. Belliard, Phys. Stat. Sol. (a) **174**, 483 (1999).
- [5] W. B. Zeper, J. A. M. Greidanus, P. F. Carcia, and C. R. Finche, J. Appl. Phys. **65**, 4971 (1989).
- [6] D. Weller, L. Folks, M. Best, E. E. Fullerton, B. D. Terris, G. J. Kusinski, K. M. Krishnan, and G. Thomas, J. Appl. Phys. **89**, 7525 (2001).
- [7] L. Belliard, J. Miltat, V. Kottler, V. Mathet, C. Chappert, and T. Valet, J. Appl. Phys. **81**, 5315 (1997).
- [8] T. H. Wu, Z. Y. Qiu, W. B. Lai, J. C. Huang, and J. C. Wu, Jpn. J. Appl. Phys. Vol. **38** (1999) pp. 1687-1690.
- [9] J. E. Davies, Olav Hellwig, Eric E. Fullerton, Greg Denbeaux, J. B. Kortright, and Kai Liu, Phys. Rev. B **70**, 224434 (2004).
- [10] C. Bran, A. B. Butenko, N. S. Kiselev, U. Wolff, L. Schultz, O. Hellwig, U. K. Rößler, A. N. Bogdanov, and V. Neu1 Phys. Rev. B **79**, 024430 (2009).
- [11] O. Hellwig, G. P. Denbeaux, J. B. Kortright, and E. E. Fullerton, Physica B **336**, 136 (2003).
- [12] R. Karplus, J.M. Luttinger, Phys. Rev. **95**, 5 (1954).
- [13] U. Hartman, Annu. Rev. Mater. Sci. (1999) 29:53-87.
- [14] O. Hellwig, A. Berger, J. B. Kortright, E. E. Fullerton, J. Mag. Mater. 319 (2007) 13-55.
- [15] C. Kooy and U. Enz, Philips Res. Rep. **15**, 7 (1960).
- [16] G. N. Phillips, K. O'Grady, Q. Meng, J. C. Lodder, IEEE Trans. Mag. **32**. 5 (1996).